





OPEN

Elongating maize root: zone-specific combinations of polysaccharides from type I and type II primary cell walls

Liudmila V. Kozlova , Alsu R. Nazipova, Oleg V. Gorshkov, Anna A. Petrova & Tatyana A. Gorshkova

The dynamics of cell wall polysaccharides may modulate the cell wall mechanics and thus control the expansion growth of plant cells. The unique composition of type II primary cell wall characteristic of grasses suggests that they employ specific mechanisms for cell enlargement. We characterized the transcriptomes in five zones along maize root, clustered the expression of genes for numerous glycosyltransferases and performed extensive immunohistochemical analysis to relate the changes in cell wall polysaccharides to critical stages of cell development in Poaceae. Specific patterns of cell wall formation differentiate the initiation, realization and cessation of elongation growth. Cell walls of meristem and early elongation zone represent a mixture of type I and type II specific polysaccharides. Xyloglucans and homogalacturonans are synthesized there actively together with mixed-linkage glucans and glucuronoarabinoxylans. Rhamnogalacturonans-I with the side-chains of branched 1,4-galactan and arabinan persisted in cell walls throughout the development. Thus, the machinery to generate the type I primary cell wall constituents is completely established and operates. The expression of glycosyltransferases responsible for mixed-linkage glucan and glucuronoarabinoxylan synthesis peaks at active or late elongation. These findings widen the number of jigsaw pieces which should be put together to solve the puzzle of grass cell growth.

The ability to expand or to elongate many times compared to the initial size is a vital property of plant cells. Cells which are capable to grow are surrounded by a thin primary cell wall (PCW). The enlargement of plant cells occurs under the action of turgor pressure and is controlled by the mechanical properties of their cell walls. Mechanical properties, in turn, depend on the cell wall composition and architecture. The mechanisms underlying the growth of plant cells have mainly been studied in dicotyledonous species and non-commelinoid monocots with type I primary cell walls (Fig. 1). Cellulose in the form of microfibrils is present in plant cell walls of all types. Type I cell walls also have pectins and xyloglucans (XyGs) as the basic constituents¹. Hydrated pectin matrix fills the spaces between cellulose microfibrils. The major part of XyGs also exists between microfibrils in a coiled conformation or interacts with them in an extended conformation. However, minor portion of XyGs is entrapped between cellulose strands². These local interactions of XyGs with cellulose named "biomechanical hotspots" were proposed to form microfibril junctions and integrate them into one load-bearing network³. The modification of these junctions by α -expansins enables the irreversible microfibril movements required for cell wall expansion². Alterations in the pectin structure are also considered a potential mechanism regulating wall expansion. Changes in cell wall hydration, the degree of cross-linking or accessibility of individual molecules to degrading enzymes are supposed to be a mechanism underlying the modulation of cell wall mechanics by pectin modifications^{4,5}.

The Poaceae family, which includes cereals, is characterized by type II primary cell walls (Fig. 1), where mixed-linkage glucans (MLGs) and glucuronoarabinoxylans (GAXs) predominate, while XyGs and pectins are present at low levels¹. MLGs, together with low substituted GAXs are thought to cover cellulose, while high substituted GAXs are localized in a space between microfibrils^{6–8}. However, in vitro studies have shown that neither arabinoxylan (AX) nor MLG serve as equivalents of either XyG or pectin in interactions with cellulose^{9,10}. An

Laboratory of Plant Cell Growth Mechanisms, Kazan Institute of Biochemistry and Biophysics, FRC Kazan Scientific Center of RAS, Kazan, Russian Federation. ✉email: kozlova@kibb.knc.ru

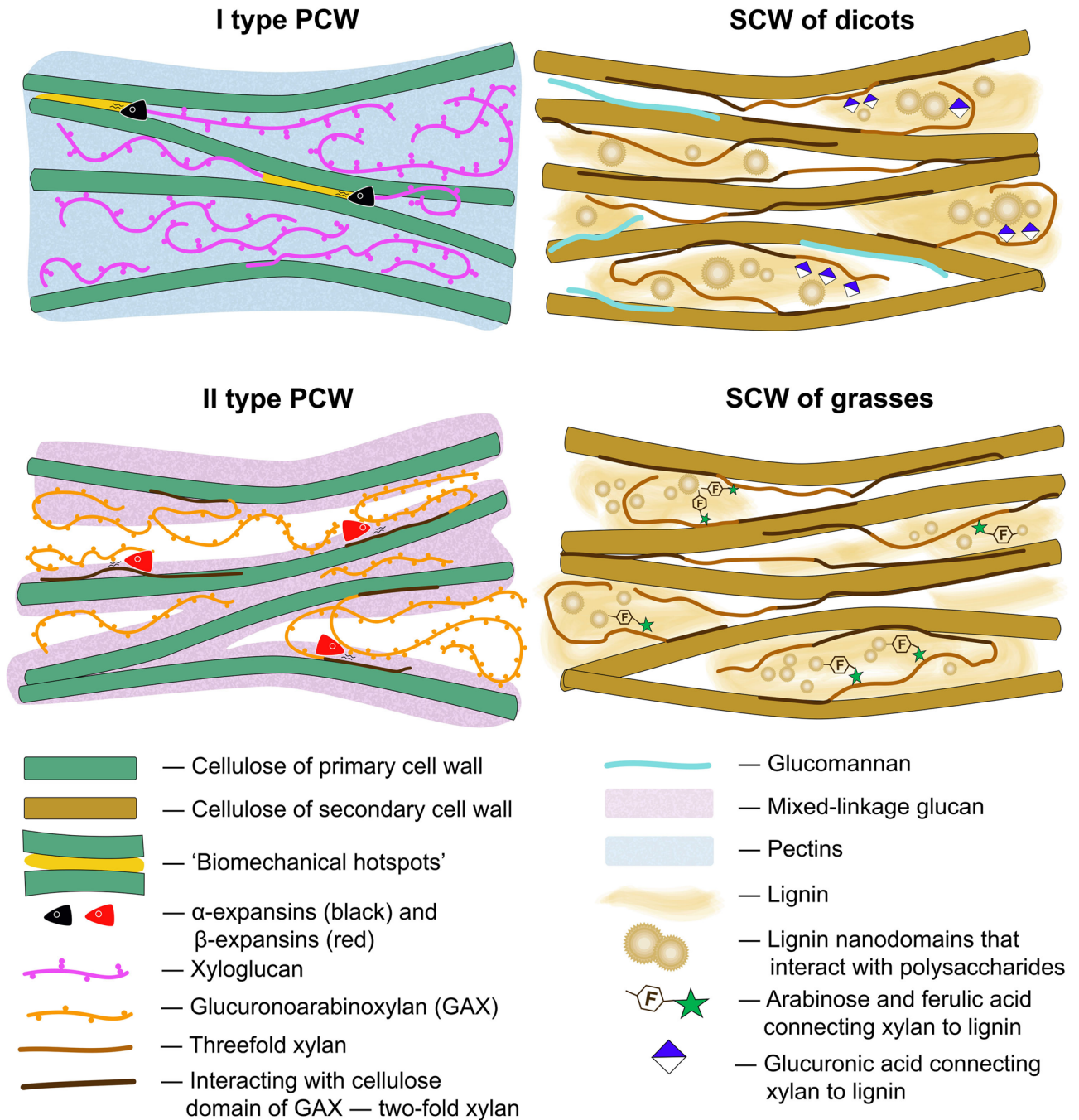


Figure 1. Different types of plant cell wall. Models may not be to scale. Based on (chronological order) Buckeridge et al.⁶, Kozlova et al.⁷, Kiemle et al.⁹, Wang et al.⁸, Simmons et al.¹⁴, Cosgrove², Kang et al.¹³, Coomey et al.¹⁵.

α -expansin treatment of grass cell walls does not cause the same loosening response as in type I cell walls^{11,12}. β -Expansins, a clade of the expansin family that has substantially evolved in grasses, interact with highly substituted GAXs and rhamnogalacturonans I (RGs-I), but not with cellulose or its contacts with low substituted AXs⁸. These observations discourage direct extrapolations of recent findings in the field of plant cell growth mechanisms obtained from dicots onto grasses.

Many specialized cells, like tracheids, vessels, fibers and sclereids, deposit thickened secondary cell wall (SCW) inside the primary cell wall. This provides additional mechanical strength to plant tissues. Usually, it happens after cessation of expansion growth because solid SCW is not extensible. However, when secondary thickenings have a spiral or annular character of depositing they do not hinder cell elongation. SCWs (Fig. 1) are composed mainly of cellulose, xylans and lignin; the latter is a branched phenolic polymer. Interaction of these three polymers occurs mainly through xylans¹³. The pattern of xylan backbone decoration determines the conformation of this polysaccharide and provides the conditions to interact either with cellulose or with lignin^{13,14}.

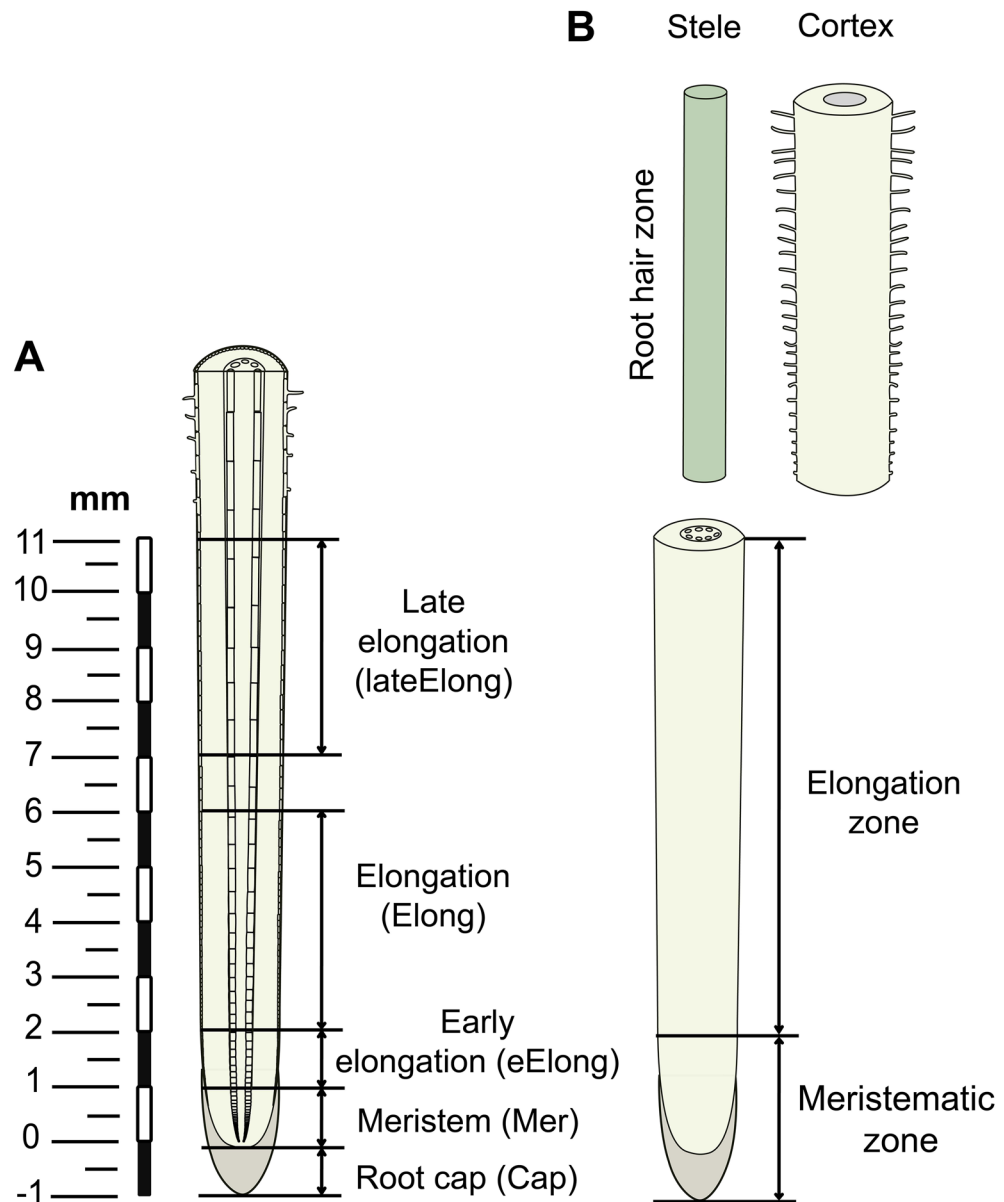


Figure 2. Schematic representation of the collection of samples from maize root in the current study (A) and for the proteome analysis reported by Marcon et al.²² (B).

Grasses have a more complex structure of both lignin and xylans¹⁵. However, the general architecture of SCW is similar in grasses and dicots (Fig. 1).

The importance of the set and structural nuances of cell wall polysaccharides for plant development is getting more and more recognized. However, the molecular details of the processes in elongating cells of grasses remain elusive and need a combination of approaches and adequate model systems for elucidation. The transcriptomic analysis is a powerful tool for identifying genes that modulate biological processes in a living cell. Over the past decade, numerous RNA-Seq and microarray analyses have been conducted on different grass organ and tissue samples to identify key participants in elongation growth. Maize internodes were among the most popular objects of such studies^{16–18}. However, the comparison between elongating and non-elongating internodes shifts the focus to genes involved in growth cessation and secondary cell wall formation. Additionally, actively growing intercalary meristems contain vascular tissues; otherwise, the meristematic regions would interrupt the transport continuity and mechanically weaken the stem¹⁹. Thus, even in its base, the internode represents a mixture of dividing and differentiated cells, which complicates the analysis.

The primary root is a more convenient model system to study elongation growth. Several zones containing cells at different stages of development can be separated from each other based on the distance from the root apex²⁰. This unique characteristic was partially employed in the large-scale analysis of transcriptomes²¹ and proteomes²² in various parts of the maize root system. Relatively large root fragments that combined several

zones were used in these studies, increasing the difficulty of distinguishing the cell division and cell elongation stages, and identifying the important processes occurring at the transition between these stages.

We have applied an RNA-Seq analysis to five zones in the apical part of maize root (before root hair emergence) to reveal key participants involved in the initiation, realization and cessation of coordinated elongation growth in a plant with type II cell walls (Fig. 2). Clustering and co-expression approaches used for genes encoding numerous glycosyltransferases (GTs) involved in the biosynthesis of cell wall polysaccharides, coupled with extensive immunohistochemical analysis to determine the distribution and dynamics of particular polysaccharide motifs, revealed several patterns of cell wall polysaccharide deposition that corresponded to important stages in cell development.

Results

Ten individual libraries of mRNAs from two biological replicates of five different samples of maize primary root were analyzed using Illumina sequencing technology. Three hundred thirty million cleaned and filtered 60 bp single-end Illumina reads with quality scores greater than Q30 were used in further analyses. Notably, 87.91% to 89.84% of the reads in each sample were mapped to the reference gene set of the version 4 maize genome, and expression values in units of TGR were calculated. The average value of Pearson's correlation coefficient for all replicates was greater than 0.95, and a clustering tree of the replicates also indicated the consistency of the data. The annotation of the *Z. mays* B73 AGPv4 (https://ensembl.gnome.org/Zea_mays) contains 44,146 genes, of which 39,324 are defined as protein-coding genes. Across all samples, 26,661 genes were identified, and 26,389 protein-coding genes were expressed with normalized TGR values > 16 at least in one sample. GTs were identified in the genome (B73 RefGen_v4) according to the presence of characteristic Pfam domains in the amino acid coding sequences (Table S1). Two hundred sixty-four genes belonging to 12 GT families and one methyl-transferase family were expressed in maize root. Their expression patterns were analyzed using a clustering analysis, and 6 clusters were identified (Table S1). The phylogenetic analysis of GTs and the comparison with known members of the same GT families in rice and *Arabidopsis* were performed to further characterize the genes and determine the clade of the family (Fig. S1–S10).

Cellulose synthase superfamily. The biosynthesis of the backbones for several cell wall polysaccharides is mediated by the enzymes encoded by members of the cellulose synthase (CesA) gene superfamily. CesA genes of maize were identified by the presence of PF03552, PF00535, and PF13632 Pfam domains in their protein sequences. The phylogenetic tree was built with known members of CesA superfamily in *Arabidopsis* and rice (Fig. S1). Maize B73 RefGen_v4 contained 53 gene models of putative CesA superfamily genes that, together with *Arabidopsis* and rice genes, were distributed in nine clades. Among the three examined species, the CslB clade was represented only by *Arabidopsis* sequences, while the CslF and CslH clades included only rice and maize genes.

Nineteen maize genes were grouped into the CesA/CesAL clade (Fig. S1). Two recent studies reported 20 members of this clade in maize^{18,23} however, both studies used older versions of the *Zea mays* genome. The new genome assembly associated two gene models, CesA9 (GRMZM2G018241) and CesAL4 (GRMZM2G150404), with the same gene Zm00001d005250. Similarly, two isoforms of CesA11, GRMZM2G037413 and GRMZM2G055795, were merged into one Zm00001d043477 gene. In contrast, Zm00001d012744, which had no associated gene models in previous genome assemblies, entered the CesA/CesAL list as CesA11a according to the phylogenetic analysis (Fig. S2). Seventeen CesA/CesAL genes were expressed in maize root with TGRs greater than 16 at least in one zone (Fig. 3).

Penning et al.¹⁸ proposed that all isoforms of genes ZmCesA1 through ZmCesA9 were involved in primary cell wall synthesis, while genes ZmCesA10 through ZmCesA12 and their isoforms were associated with secondary cell wall biosynthesis. ZmCesA1, 2, 4, 6, 8a/b and 9 displayed similar expression profiles along the root length. Transcripts of these genes were relatively abundant in the meristem zone. Four- to five-fold up-regulation was characteristic of these genes in the early elongation zone, with further increase in the elongation zone and two-fold down-regulation at the late elongation stage. According to the proteomic study performed by Marcon et al.²², corresponding proteins were present in the meristematic region of maize seedling primary root and accumulated during elongation. Both stele and cortex tissues in the root hair region of young maize root were characterized by high levels of these cellulose synthases²². These features of the transcription and translation of particular cellulose synthase genes probably reflect the high demand for new cell wall material by rapidly elongating cells. The six mentioned cellulose synthases were co-expressed with each other, with correlation coefficients greater than 0.95. They were used as the bait genes for the co-expression analysis to reveal other GTs governed by the same regulatory pattern (Table S1, net_pcw column, Figs. 3–6).

The ZmCesA10–12 genes were expressed at low levels in the root cap, meristem and early elongation zone. Significant increases in the levels of their transcripts occurred in the elongation zone, with further increases in the TGR values in the late elongation zone. High levels of the corresponding proteins were detected in the stele of the root hair region of maize root²². A virtual absence of certain transcripts and proteins at the earlier stages of cell development, transcriptional up-regulation in the elongation zone that peaked at the stage of late elongation, and the high levels of proteins in the stele of the root hair region corresponded to the development of the vascular system and secondary cell wall thickening in maize root. Four isoforms of maize CesAs (10, 11, and 12a/b) were co-expressed, with correlation coefficients greater than 0.95, and were selected as bait genes to build the co-expression network related to secondary cell wall biosynthesis (Table S1, net_scw column; Figs. 3–6).

Members of the cellulose synthase-like H, F and J clades of the CesA superfamily mediate MLG synthesis in grasses and heterologous expression systems²⁴. According to the phylogenetic tree, seven sequences of maize

genes were grouped with rice CslFs, and one with rice CslHs genes (Fig. S1). No representatives of CslJ subfamily were found.

Two maize orthologues of the rice CslF6 gene (Zm00001d024531 and Zm00001d049510) exhibited the highest TGRs in the active elongation zone and were co-expressed ZmCesAs, which are predicted to be involved in primary cell wall formation (Fig. 3 and Table S2). Another member of the CslF clade (Zm00001d021736, the orthologue of rice and barley CslF3) was up-regulated in the meristem and early elongation zone. This GT was recently shown to possess novel activity, mediating the synthesis of glucoxytan²⁵. Protein products of this gene were detected in maize root segments before, but not after, root hair initiation²².

Glucuronoarabinoxylan (GAX) synthesis. GAXs are the major noncellulosic polysaccharides present in the type II primary walls. The synthesis of its β -1,4-xylan backbone is mediated by a complex of three proteins. Two of these proteins (IRX9 and IRX14) represent the GT43 family (Fig. S3), and the other (IRX10) belongs to a separate clade of the GT47 family (Fig. S4). Xylosyl-transferase activity in vitro has only been observed for IRX10^{26,27}. IRX9 and IRX14 are believed to function as structural components of the xylan synthase complex with no catalytic activity *per se*²⁶.

Maize RefGen_v4 contains 51 genes encoding proteins with the predicted PF03016 Pfam domain, which is the signature of the GT47 family. Four of them were shorter than 270 amino acids and were excluded from further analysis. The phylogenetic tree with *Arabidopsis* GT47 members was built to identify maize orthologues of AtIRX10 and AtIRX10L (Fig. S4). The IRX10 clade of GT47 included ten paralogous genes of maize. All were expressed in maize root, with the highest TGR values observed in the zones of active or late elongation (Fig. 3). Three isoforms of ZmIRX10 (Zm00001d042281, Zm00001d009465, and Zm00001d042279) were co-expressed with primary cell wall CesAs, and two others (Zm00001d042276 and Zm00001d011959) were co-expressed with secondary cell wall CesAs (Fig. 3). The GT43 family is represented in the maize genome by 15 members encoding proteins containing the PF03360 domain (Fig. S3). All these genes were expressed (Fig. 3). Ten belonged to either primary or secondary cell wall-related co-expression networks.

The GAX backbone can be decorated with arabinose, glucuronic acid, xylose or oligosaccharide chains. The attachment of arabinosyl and xylosyl residues to the GAX molecule is mediated by GTs of the GT61 family^{28,29}, while GT8 members are required for the glucuronosyl substitution of the xylan backbone³⁰.

The GT61 family has been subdivided into several clades with specific characterized members (Fig. S5). Clade A contains maize orthologues for rice OsXAT2 (Zm00001d053282) and OsXAT3 (Zm00001d046005), as well as wheat TaXAT1 (Zm00001d036122). XATs are xylan α -1,3-arabinofuranosyl-transferases²⁸. The majority of genes in the XAT subgroup of the maize GT61 family were expressed with the maximum TGR values in the early elongation or elongation zones (Fig. 4).

One additional characterized member of GT61 clade A is OsXAX1. The enzyme encoded by this gene adds β -1,2-xylose to the α -1,3-arabinose side-chain of the xylan backbone²⁹. Three maize genes are present on the branch of GT61 tree that contains OsXAX1. Zm00001d046004 had highest TGR value among all genes belonging to this subclade. Two other genes on the same branch (Zm00001d054066 and Zm00001d014965) were co-expressed with primary or secondary cell wall-related CesAs, respectively (Fig. 4).

Another member of GT61 clade A, XYXT1, functions in rice as a xylosyl-transferase attaching β -1,2-xylosyl side-chains onto the xylan backbone³¹. The maize orthologue of OsXYXT1 (Zm00001d014721) had highest TGR values in the early elongation and elongation zones, and was significantly down-regulated in the late elongation zone of maize root (Fig. 4).

Clade B of the GT61 tree contains AtMUCI21 and six genes of maize that were expressed in the primary root. AtMUCI21 was characterized as a β -1,2-xylosyl-transferase, a xylan branching enzyme of *Arabidopsis* seed mucilage³². Three maize members of the GT61 clade B were predominantly expressed in the elongation zone, while two others were expressed in the late elongation zone of maize root.

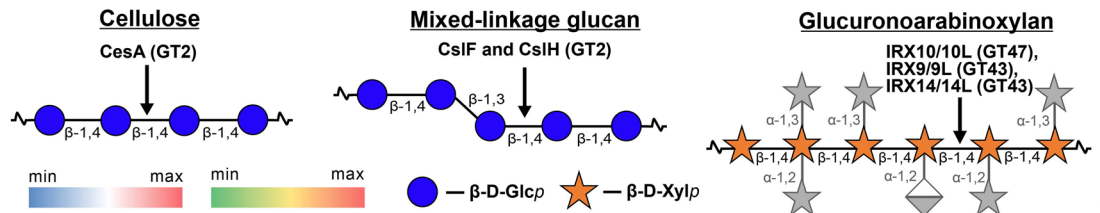
The enzymes known to mediate the attachment of α -1,2-GlcA side-chains onto the xylan backbone in dicots^{33,34} represent a separate clade of the GT8 family (Fig. S6). Five of these genes were expressed in maize primary root, with the maximum of TGR values in either the active elongation or late elongation stages.

Thus, two different sets of GTs, both of which are sufficient for the production of highly substituted xylans, are expressed in maize primary root. Genes and proteins of these enzymes appear along the root length in a manner corresponding to primary and secondary cell wall biosynthesis.

Xyloglucan (XyG) synthesis. XyGs consist of a backbone of 1,4-linked β -D-glucosyl residues, some of which are substituted at O(6) with an α -D-xylosyl residue. Further substitution of xylose with galactose or fucosyl-galactose may occur in cell walls of Poales^{35,36}.

The formation of the XyG backbone is catalyzed by members of the CslC clade of the GT2 family³⁷. CslC4 of *Arabidopsis* induced XyG backbone synthesis in heterologous systems³⁸. The maize genome contains eight members of the CslC clade (Fig. S1); all eight genes were expressed in maize root (Fig. 5). Two orthologues of the *Arabidopsis* CslC5 gene (Zm00001d049336 and Zm00001d024178) were expressed at high levels, with maximum TGR values observed in the root cap and meristem (Fig. 5). A greater than 25-fold decrease in transcript abundance was observed in the zone of active elongation. Proteins encoded by these genes were expressed at the highest levels in the meristematic region of maize root²². Zm00001d049336 is also the orthologue of OsCslC3, which is predicted to function as a XyG backbone synthase in rice³⁶. This gene was chosen as the bait in the co-expression analysis to identify other participants in XyG synthesis in maize (Fig. 5 and Table S1, xyg_net column).

The XyG backbone is decorated by xylose residues. In *Arabidopsis*, the attachment of xylose is catalyzed by members of the GT34 family XXT1, 2, 4 and 5^{39,40}. The maize genome possesses 18 genes containing the Pfam domain (PF05637) characteristic of GT34. Twelve representatives of XXT clade (Fig. S7) were expressed (Fig. 5).



GeneID	Total Gene Reads					Penning et al., 2019	Relative protein abundance, Marcon et al. (2015)				
	Cap	Mer	eElong	Elong	lElong		Cap+Mer +eElong	Elong+ lElong	Cortex RH	Stele RH	Whole Root
CesA/CesAL											
Zm00001d019317	1936	3977	27460	44727	17672	CesA8b	176	985	1416	1386	1865
Zm00001d005250	1400	4714	19762	26713	12489	CesA9	309	934	1295	1071	1605
Zm00001d037636	1061	4451	23130	26186	11794	CesA2	359	1571	2783	2146	3032
Zm00001d019149	634	2946	16368	20564	9093	CesA4	132	714	1587	890	1139
Zm00001d009795	769	2262	9670	12780	5942	CesA1	239	813	1491	1279	1773
Zm00001d005478	1150	1386	7241	11465	4786	CesA8a	62	419	540	311	403
Zm00001d034770	1056	1822	5501	8344	6061	CesA6	177	437	298	332	200
Zm00001d019507	428	547	2524	5474	13923	CesA7a	7	61	813	609	925
Zm00001d043477	4	9	284	3269	4065	CesA11b	0	0	121	1415	95
Zm00001d032776	1	3	185	2327	2894	CesA10	109	148	175	1291	353
Zm00001d005451	359	276	429	1898	6334	CesA7b	0	35	52	79	97
Zm00001d034553	624	519	476	1561	1370	CesA5	74	57	116	46	3
Zm00001d020531	12	13	52	1260	1445	CesA12a	4	19	63	696	139
Zm00001d046127	58	176	921	1186	611	CesAL1	no data	no data	no data	no data	no data
Zm00001d005775	0	0	29	1138	1612	CesA12b	0	0	97	896	84
Zm00001d039660	537	342	257	260	504	CesA3	2	31	14	40	0
Zm00001d046691	145	117	114	199	172	CesAL3	no data	no data	no data	no data	no data
Zm00001d012744	0	0	2	0	24		no associated gene in RefGen_v3				
CSLF											
Zm00001d024531	427	1188	11585	22128	9359	CsiF2	0	184	412	433	152
Zm00001d049510	832	1843	14040	17351	11185	CsiF4	4	314	211	523	332
Zm00001d021731	112	264	947	1546	2219	CsiF3	0	34	78	12	0
Zm00001d021736	193	1473	2166	375	88	CsiF7	42	193	0	0	18
Zm00001d006571	15	70	121	28	1	CsiF8	no data	no data	no data	no data	no data
Zm00001d021732	33	1	0	5	9	CsiF1	no data	no data	no data	no data	no data
Zm00001d032909	0	0	0	3	57	CsiF6	no data	no data	no data	no data	no data
GT47, IRX10 clade											
Zm00001d038905	261	455	1625	3033	3198	IRX10-1d	0	192	150	439	113
Zm00001d042276	9	19	677	2959	2841	IRX10-1a	0	0	13	165	0
Zm00001d042281	160	841	2099	2680	1387	IRX10-1h	13	188	50	69	0
Zm00001d009465	235	355	938	1577	1391		no associated gene in RefGen_v3				
Zm00001d042279	294	456	1505	1328	764	IRX10-1f	23	62	89	78	35
Zm00001d011959	65	87	303	821	741	IRX10-1c	0	0	0	106	0
Zm00001d003878	489	498	673	733	1096	IRX10-1g	67	33	9	9	17
Zm00001d011964	87	271	501	615	637	IRX10-1i	no data	no data	no data	no data	no data
Zm00001d013199	22	34	61	116	111	IRX10-1b	no data	no data	no data	no data	no data
Zm00001d051954	3	5	14	65	33		no associated gene in RefGen_v3				
GT43											
Zm00001d010976	847	1832	3856	6056	5242	IRX9c	49	190	355	262	77
Zm00001d002064	56	427	2440	4070	1820	IRX14d	0	33	61	97	29
Zm00001d014525	994	1596	2722	4029	4221	IRX14a	58	119	103	402	280
Zm00001d036543	571	883	1694	2268	2768	IRX14b	101	200	165	624	162
Zm00001d026460	55	122	979	2089	1576		no associated gene in RefGen_v3				
Zm00001d009539	357	577	1518	2010	1495	IRX9Ld	no data	no data	no data	no data	no data
Zm00001d028725	34	54	815	1991	1555	IRX9b	0	25	12	97	10
Zm00001d047750	75	92	441	815	877	IRX9a	0	12	18	142	10
Zm00001d043879	36	88	217	659	865	IRX9Lc	no data	no data	no data	no data	no data
Zm00001d004545	67	65	184	311	338		no associated gene in RefGen_v3				
Zm00001d024934	50	28	130	279	354	IRX9Lb	no data	no data	no data	no data	no data
Zm00001d038981	140	146	186	266	329	IRX9Le	no data	no data	no data	no data	no data
Zm00001d008250	26	13	41	166	378	IRX9La	0	0	0	0	0
Zm00001d007231	7	3	41	102	232	IRX9d	no data	no data	no data	no data	no data
Zm00001d035494	94	60	78	88	45		no associated gene in RefGen_v3				

◀ **Figure 3.** Expression level (TGR, red-blue heat map) and relative protein abundance (averaged and normalized total spectral counts²², red-green heat map) of ZmCesA/CesAL, ZmCslFs and genes encoding members of the xylan backbone synthase complex in various zones of maize root. Heat map color coding is applied separately to each gene subgroup. The underlined gene names indicate the baits for co-expression analysis. The genes co-expressed with maize primary cell wall CesAs are labelled in blue, and genes co-expressed with secondary cell wall CesAs are labelled in red. Annotations are based on the study by Penning et al.¹⁸, and are obtained by matching of the RefGen_v3 and RefGen_v4 gene models. The annotations shown in blue and in red are CesAs assigned to primary and secondary cell wall formation, respectively, by Penning et al.¹⁸. Cap—root cap, Mer—meristem, eElong—early elongation zone, Elong—zone of active elongation, lElong—zone of late elongation before root hair initiation, and RH—root hair zone. No data, i.e., no corresponding peptides were obtained from any of the studied root samples²².

The maximum levels of the transcripts of almost all GT34 members were observed in the root cap or meristem zone of maize root. Expression decreased at later stages of cell development. Five of these genes were co-expressed with ZmCslC5c (Fig. 5 and Table S1). Proteins of the GT34 family were mainly detected in the elongating part of maize root, and rarely in the root hair region.

Xylose residues attached to the XyG backbone may be further substituted at the O(2) position with galactose. Two GTs of the GT47 family, MUR3 and XLT2, are predicted to be involved in XyG galactosylation in *Arabidopsis*⁴¹. Representatives of the GT47 family possess various activities, and the family is divided into several clades (Fig. S4). The MUR3/XLT2 clade contained 14 genes expressed in maize root. The vast majority of these genes were expressed with the highest TGR values in root cap and meristem zones. A recent study of *Sorghum* revealed two proteins functioning as the XyG galactosyl-transferases⁴². The Zm00001d032794 gene is an orthologue of one of these genes in maize. This gene and two other members of the MUR3/XLT2 clade were co-expressed with ZmCslC5c (Fig. 5).

Fucose-containing side-chains of XyG are barely detectable in Poaceae species³⁵. However, fucogalactoxyloglucans were recently identified in young tissues of rice³⁶. XyG fucosylation is catalyzed by members of the GT37 family⁴³. Nineteen genes belonging to this family were recognized in the RefGen_v4 maize genome, according to the presence of the PF03254 Pfam domain. Fourteen of these genes were expressed in analyzed root zones, and among them, four orthologues of AtFUT1 (Zm00001d020721, Zm00001d003510, Zm00001d044933, and Zm00001d044872) known to be involved in fucosylation of XyGs in *Arabidopsis*⁴⁴ and one orthologue of rice OsFUT1 (Zm00001d052168) were detected. All five presented the highest TGR values in the root cap zone, and corresponding proteins were observed only in the meristematic part of maize root (Fig. 5).

Pectin synthesis. Pectins are minor components of type II cell walls, comprising only 2–10% of the dry mass⁴⁵. Homogalacturonan (HG) usually is the most abundant pectic polysaccharide. It consists of an α -1,4-linked D-galacturonic acid (GalA) backbone, which is synthesized by HG galacturonosyl-transferases (GAUTs)^{46–48}. GAUTs belong to the GT8 family (PF01501), which also includes xylan α -glucuronyl-transferases (GUXs) and glucoside α -1,3-galactosyltransferases (GATLs) participating in GAX and AGP synthesis, respectively (Fig. S6).

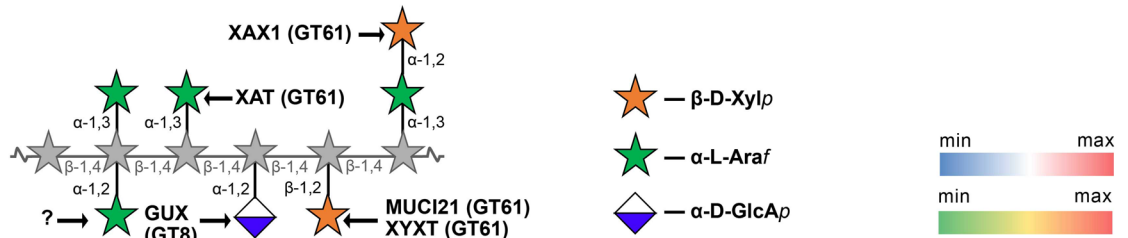
Forty-seven members of the GT8 family were identified in the fourth version of the maize genome, although three of these genes are too short to encode active enzymes. Twenty-four of these genes belong to the GAUT clade (Fig. S6). The vast majority of GAUTs exhibited maximum TGR values in the early elongation or elongation zone (Fig. 6). Corresponding proteins were not detected at high levels, but were mainly observed in the elongating part of the root in the study by Marcon and colleagues²².

HG is synthesized in a highly methyl-esterified form and is postulated to lose ester groups during the elongation growth of cells⁵. The attachment of methyl groups is mediated by methyl-transferases belonging to the Methyl_Transf_29 family possessing the characteristic PF03141 Pfam domain. Fifty-seven genes encoding proteins with this domain were identified in maize RefGen_v4, 41 of which were expressed in maize primary root. AtQUA2 is characterized on the protein level as pectin-methyl-transferase in *Arabidopsis*^{49,50}. Two orthologues of AtQUA2 in maize (Zm00001d052213 Zm00001d031670) were expressed with high TGR values; however, no corresponding proteins were detected in a proteomic study²² (Fig. 6).

The backbone of rhamnogalacturonan I (RG-I) is composed of repeating diglycoside 2- α -L-Rhap-1,4- α -D-GalpA-1 units. Recently, members of GT106 (RRT clade), which were previously annotated as fucosyl-transferases, were shown to catalyze rhamnose attachment to the RG-I backbone acceptor⁵¹. The RRT clade is represented by eight genes in the maize genome (Fig. S8). All of these genes were expressed in the primary root. Only the protein encoded by Zm00001d037367 was detected²². This gene and two other members of this clade belonged to the co-expression network of CesAs genes responsible for primary cell wall formation.

The RG-I backbone can be substituted at the (O)2 position of rhamnosyl residues. Side-chains usually are represented by β -1,4-D-Galp or α -1,5-L-Araf oligosaccharides. The synthesis of β -1,4-galactan in *Arabidopsis* is mediated by the GT92 family member AtGALS1⁵². Three orthologues of this gene are present in the *Zea mays* genome. All of these genes were expressed in the apical part of maize root. Other members of the GT92 family exhibited low similarity with GALS1. No corresponding proteins were detected²². However, two of the three maize GALS1 orthologues were co-expressed with primary cell wall CesAs (Fig. 6).

Another type of side-chains for RG-I is α -1,5-L-arabinan, the synthesis of which is catalyzed by AtARAD1 in *Arabidopsis*⁵³. This enzyme belongs to the GT47 family (clade C) (Fig. S4). Eight members of this clade were expressed in the maize primary root. The orthologue of AtARAD1 (Zm00001d021821) presented higher TGR values in the root cap, meristem and early elongation zone (Fig. 6). However, corresponding proteins were detected only in the cortex of the root hair region²².



GeneID	Total Gene Reads					Penning et al., 2019	Relative protein abundance, Marcon et al., 2015				
	Cap	Mer	eElong	Elong	lElong		Cap+Mer +eElong	Elong+ lElong	Cortex RH	Stele RH	Whole Root
GT61											
Clade A, subclade XAT											
Zm00001d053282	956	3016	6986	3037	664	XYLTa	383	1534	72	77	109
Zm00001d046005	228	659	4349	6424	2638		no data	no data	no data	no data	no data
Zm00001d054000	217	357	1219	943	459	GT61-12	no data	no data	no data	no data	no data
Zm00001d015186	518	933	2602	2708	1961	GT61-11	56	244	172	0	163
Zm00001d014722	125	343	1702	2877	2385	GT61-9	0	11	41	77	12
Zm00001d040075	322	613	893	2996	3874	XYLTc	6	279	540	27	8
Zm00001d040059	1207	1245	2404	1391	853	GT61-6	3	35	0	0	0
Zm00001d042490	1418	1049	1523	598	634	GT61-8	178	438	451	55	108
Zm00001d008526	835	360	86	14	6	GT61-4	no data	no data	no data	no data	no data
Zm00001d036122	182	115	258	304	362	GT61-7	0	18	107	0	16
Zm00001d008495	148	93	75	97	297	GT61-5	0	0	17	0	0
Zm00001d008496	19	6	2	2	2		no data	no data	no data	no data	no data
Zm00001d040071	20	0	0	0	2	XYLTb	no data	no data	no data	no data	no data
Clade A, subclade XAX											
Zm00001d046004	38	66	1585	5678	4205	GT61-19	4	69	571	23	48
Zm00001d054066	544	947	2789	3642	1652	no associated gene in RefGen_v3					
Zm00001d040067	72	44	870	2930	2067	GT61-15	0	69	238	0	7
Zm00001d014965	8	8	108	874	1413	GT61-20	0	0	37	631	119
Zm00001d040066	12	38	422	854	264	GT61-18	4	47	129	4	51
Zm00001d045972	36	4	131	503	241	GT61-14	0	0	0	0	0
Zm00001d016544	133	209	153	150	228	GT61-13	no data	no data	no data	no data	no data
Zm00001d040060	223	262	227	35	6	GT61-16	no data	no data	no data	no data	no data
Zm00001d040064	360	232	64	7	10	GT61-17	no data	no data	no data	no data	no data
Zm00001d008494	1037	354	76	2	1		5	11	0	0	0
Clade A, subclade XYXT											
Zm00001d014721	279	503	1256	1137	214	GT61-3	no data	no data	no data	no data	no data
Zm00001d030391	299	812	685	184	24	XYLTd	0	77	0	0	6
Zm00001d046093	287	584	576	59	0	XYLTg	no data	no data	no data	no data	no data
Zm00001d037041	258	353	500	30	4		0	5	0	0	0
Zm00001d046091	835	516	64	0	0	XYLTe	no data	no data	no data	no data	no data
Clade B, MUCI											
Zm00001d038105	182	482	1563	3130	1657	MUCI21e	0	16	0	0	0
Zm00001d022380	203	71	194	1069	500	MUCI21b	0	0	0	0	0
Zm00001d010466	229	265	722	1006	576	MUCI21d	no data	no data	no data	no data	no data
Zm00001d009328	126	18	39	456	906	MUCI21a	no data	no data	no data	no data	no data
Zm00001d007076	23	6	12	129	272	MUCI21c	no data	no data	no data	no data	no data
Zm00001d040214	165	8	5	1	3	GT61-2	0	0	0	0	0
Clade C, XYLT											
Zm00001d031415	314	519	584	231	145	XYLTf	0	0	0	4	0
GT8											
GUX clade											
Zm00001d042627	1263	1345	3508	4427	4092	GUX1d	5	37	0	6	20
Zm00001d012224	883	842	1637	1677	1307	GUX1b	5	4	7	0	4
Zm00001d027938	2	0	15	1344	4208	GUX2	0	0	4	28	0
Zm00001d038229	23	8	40	701	1803	GUX1a	0	0	0	0	0
Zm00001d016806	2	0	0	13	116	GUX1e	no data	no data	no data	no data	no data

Figure 4. Expression level (TGR, red-blue heat map) of genes potentially involved in GAX backbone decoration in maize root and relative levels of the corresponding proteins (averaged and normalized total spectral counts²², red-green heat map). Heat map color coding is applied separately to each gene subgroup. The genes co-expressed with maize primary cell wall CesAs are labelled in blue, and genes co-expressed with secondary cell wall CesAs are labelled in red. Annotations are based on the study by Penning et al.¹⁸, and are obtained by matching the RefGen_v3 and RefGen_v4 gene models. Cap—root cap, Mer—meristem, eElong—early elongation zone, Elong—zone of active elongation, lElong—zone of late elongation before root hair initiation, and RH—root hair zone. No data, i.e., no corresponding peptides were detected in any of the studied root samples²².

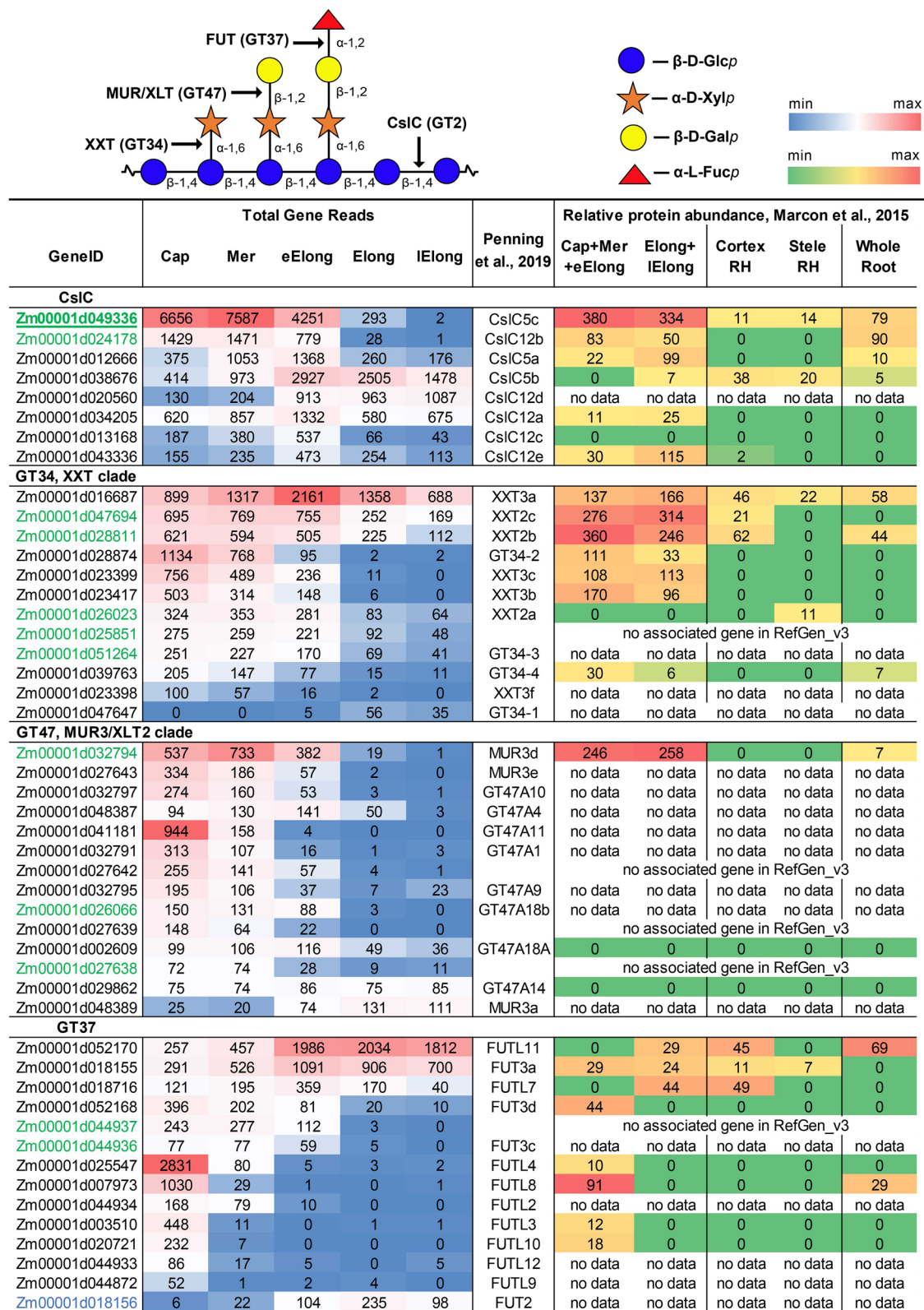
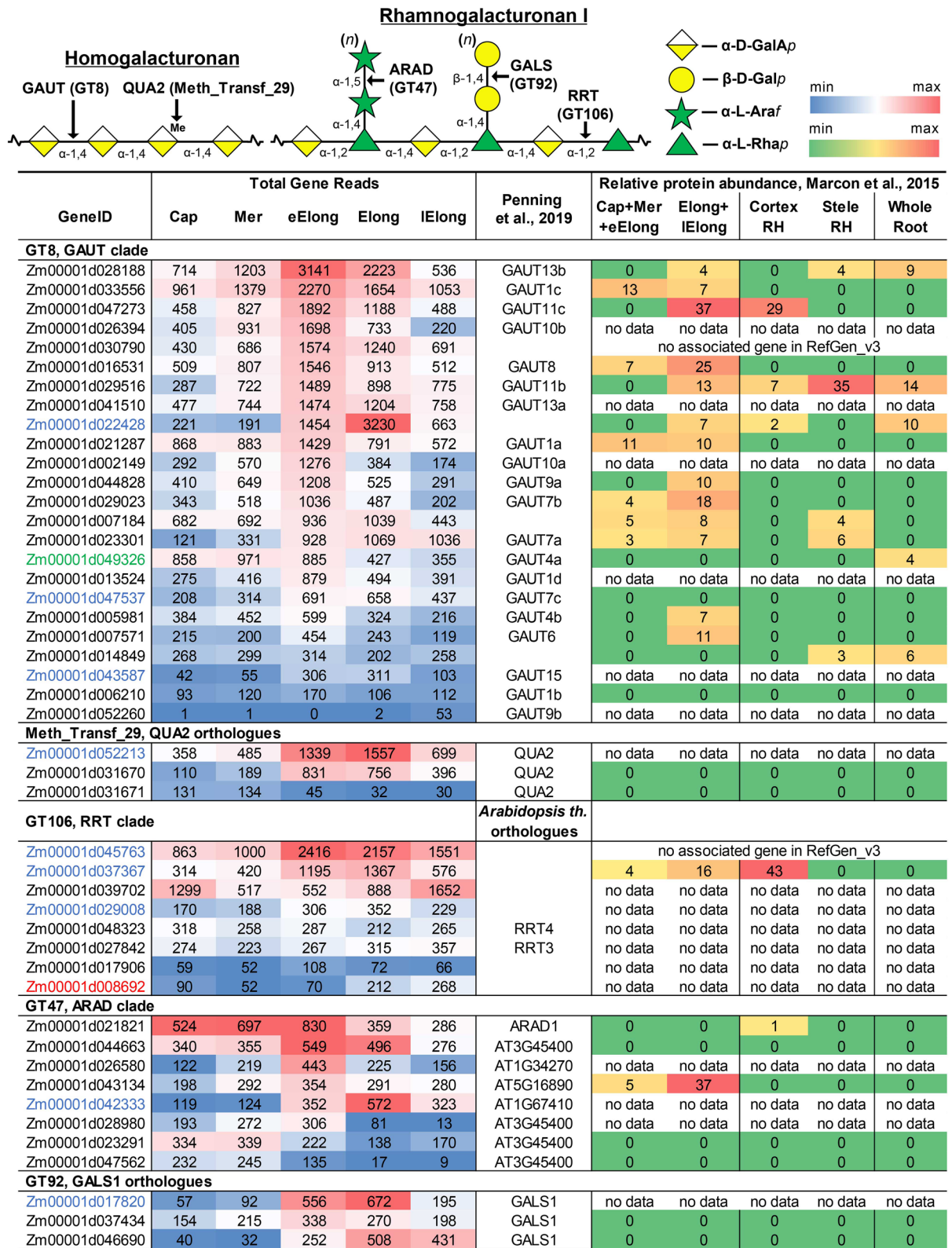


Figure 5. Expression level (TGR, red-blue heat map) and relative protein abundance (averaged and normalized total spectral counts²², red-green heat map) of genes potentially involved in XyG synthesis in maize root. Heat map color coding is applied separately to each gene subgroup. The gene co-expressed with maize primary cell wall CesAs is labelled in blue. Green indicates genes co-expressed with ZmCslC5c (underlined) and displaying a correlation coefficient greater than 0.95. Annotations are based on the study by Penning et al.¹⁸, and are obtained by matching the RefGen_v3 and RefGen_v4 gene models. Cap—root cap, Mer—meristem, eElong—early elongation zone, Elong—zone of active elongation, lElong—zone of late elongation before root hair initiation, and RH—root hair zone. No data, i.e., no corresponding peptides, were detected in any of the studied roots²².



◀ **Figure 6.** Expression level (TGR, red-blue heat map) and relative protein abundance (averaged and normalized total spectral counts²², red-green heat map) of genes potentially involved in HG and RG-I biosynthesis in maize root. Heat map color coding is applied separately to each gene subgroup. The genes co-expressed with maize primary cell wall CesAs are labelled in blue, and genes co-expressed with secondary cell wall CesAs are labelled in red. Green indicates genes co-expressed with ZmCslC5c presenting correlation coefficients greater than 0.95. Annotations are based on the study by Penning et al.¹⁸, and are obtained by matching the RefGen_v3 and RefGen_v4 gene models Cap—root cap, Mer—meristem, eElong—early elongation zone, Elong—zone of active elongation, lElong—zone of late elongation before root hair initiation, and RH—root hair zone. No data, i.e., no corresponding peptides, were detected in any of the studied root samples²².

Immunohistochemistry. The presence of transcripts and proteins of GTs essential for the synthesis of a particular polysaccharide does not indicate that this polymer is indeed produced. We performed immunohistochemical analysis with a set of monoclonal antibodies to trace the dynamics of cell wall polysaccharides during the elongation growth of maize root.

Calcofluor White stained cell walls in maize root evenly in the meristem, early elongation and elongation zones (Fig. 7, Calcofluor White). Yellow coloration appeared in the vascular parenchyma in the late elongation zone, indicating its lignification. Brighter staining of the vascular ring corresponded to secondary cell wall thickening (Fig. 7).

BG1 and AX1 antibodies, which bind MLGs⁵⁴ and AXs⁵⁵, respectively, labelled maize cell walls in all investigated zones (Fig. 7, BG1 and AX1). However, their labelling was weaker in meristem region. The rhizodermis was only labelled by the AX1 antibody in the late elongation zone. The LM27 antibody recognizing grass heteroxylans⁵⁶ did not label meristematic cells. At the stage of early elongation, it bound the rhizodermis and outer cell layer of the cortex. A similar pattern was observed in the elongation zone. Labelling was increased centripetally in the late elongation zone and observed in several layers of the cortex (Fig. 7, LM27). The LM28 antibody specific for glucuronoxylans⁵⁶ labelled all tissues except rhizodermis. The preference for binding to stele tissues was observed in the early elongation, elongation and late elongation zones (Fig. 7, LM28). The LM11 antibody is often used to detect secondary cell wall xylans. It was raised against xylooligosaccharides⁵⁷ and probably requires a less substituted backbone fragment in contrast to other anti-GAX probes used in the current study. The LM11 antibody labelled vascular tissues in the elongation and late elongation zones. Brighter labelling was also observed in the rhizodermis in the late elongation zone (Fig. 7, LM11).

The epitope of LM25, the antibody specific for galactoxyloglucans⁵⁸, was detected at relatively high levels in the meristematic region of maize root and root cap cells, and in the slime produced by these cells. The labelling intensity increased in the early elongation zone and then decreased in the elongation and late elongation zones. However, the root slime in these zones still bound the antibody (Fig. 7, LM25). A similar pattern of labelling was observed with another xyloglucan-specific antibody, LM15 (data not shown).

LM19 and LM20 antibodies are used to detect unesterified and methyl-esterified HGs, respectively⁵⁹. LM20 epitopes were present only in the meristematic region, and the labelling became weaker in subsequent zones. In contrast, LM19 labelling became more intense in the early elongation zone. Rhizodermis or root slime did not possess the epitopes for the LM19 antibody. Elongation and late elongation zones were characterized by stronger labelling with the LM19 antibody in the root stele. A higher level of these epitopes was observed in the vascular parenchyma and phloem/protoxylem ring in the late elongation zone (Fig. 7, LM20 and LM19).

The RU2 antibody recognizes the backbone of RG-I⁶⁰. The root cap cells and root slime were labelled by this antibody. Cell walls in cell corners of middle cortex and pith were strongly labelled throughout root development (Fig. 7, RU2). Three antibodies specific for RG-I side-chains were also used. 1,4-Galactans (LM5⁶¹) were detected in root cap cells or slime and root meristematic tissues, excluding the rhizodermis. The early elongation zone possessed lower levels of epitopes for the LM5 antibody, while a gradual increase in the labelling intensity was observed in stele tissues in the elongation and late elongation zones. Phloem cells were enriched in LM5 epitopes (Fig. 7, LM5). The recently developed LM26 antibody marks β -1,4-galactan branched at the O(6) position with another galactosyl residue⁶². LM26 labelling was much stronger than LM5 labelling (Fig. 7, LM26). All tissues analyzed at all of the developmental stages possessed epitopes for the LM26 antibody. The staining with the LM6 antibody (α -1,5-arabinan⁶³), was also intense. The antibody was distributed evenly in all tissues and in all zones of maize root (Fig. 7, LM6).

Major patterns of cell wall formation. Transcriptomic data for all GTs recognized in the maize genome were subjected to a cluster analysis. Six clusters were revealed, four of which were the most populated (Fig. 8 and Table S1). Cluster 1 included genes expressed at high levels in the root cap and meristem zone and at lower levels in subsequent zones of maize root. It was enriched with numerous GTs potentially involved in XyG biosynthesis. According to the data reported by Marcon et al.²², corresponding proteins were observed in maize root before, but rarely after, root hair initiation (Fig. 8). XyG epitopes were present in the cell walls of the meristem and early elongation zone (Fig. 7, LM25).

Members of another cluster displayed peak expression in the early elongation zone. This cluster was enriched with representatives of GT8 (GAUT clade), GT31 and GT2 (ZmCslF3 and ZmCslF7), putative mediators of HG backbone, arabino-galactan protein and glucoxylan synthesis, respectively. Proteins encoded by these genes were present in the apical part and elongation zone of maize root, but not in the root hair region²² (Fig. 8). Esterified HGs disappeared from root sections at the beginning of elongation (Fig. 7, LM20), while unesterified pectins persisted in sections throughout development (Fig. 7, LM19). Polysaccharide synthases belonging to this cluster may have specific roles in the transition to elongation.

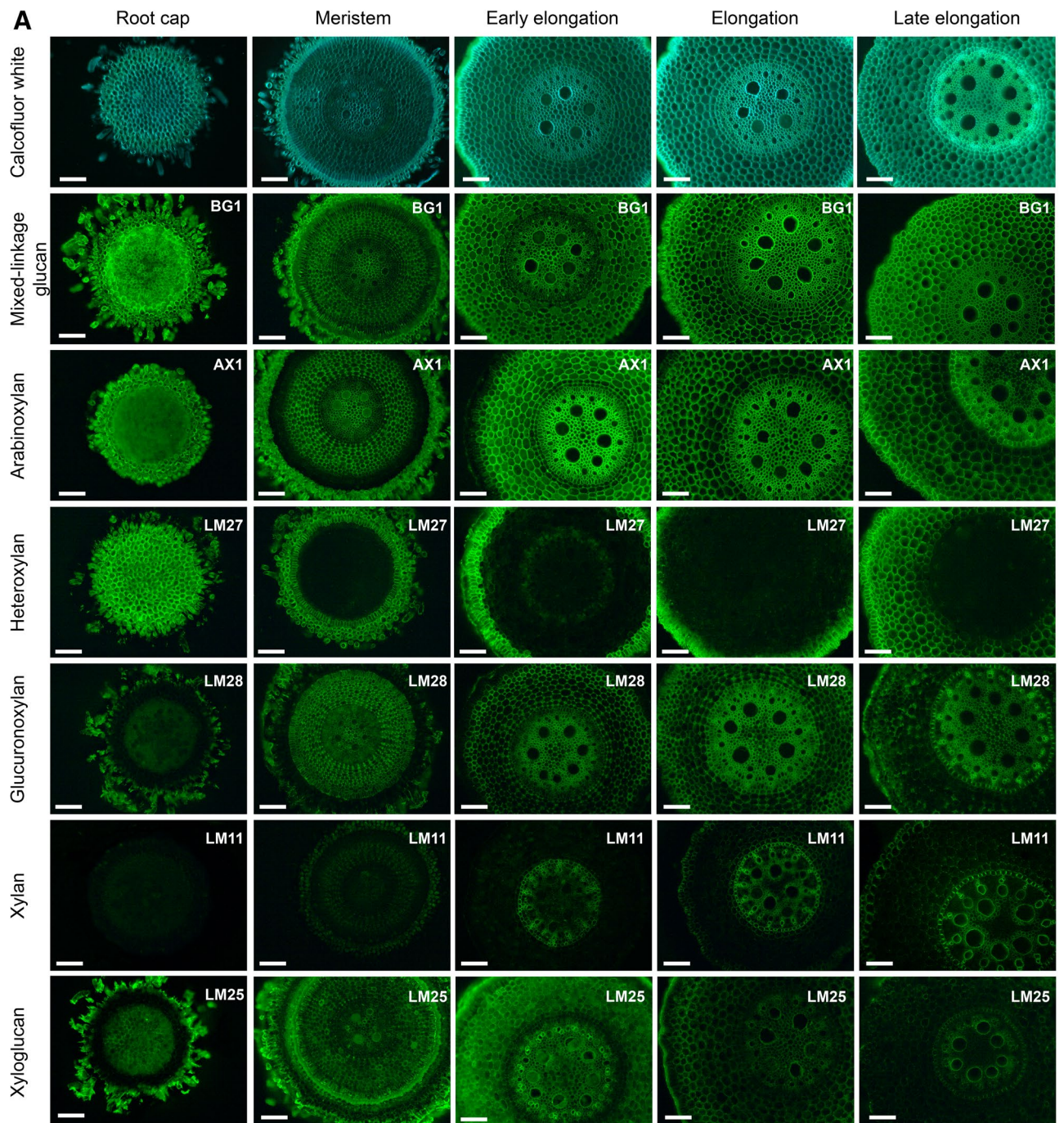


Figure 7. Fluorescence micrographs of maize root sections stained with Calcofluor White and immunolabelled by BG1 (mixed-linkage glucan), LM25 (galactoxyloglucan), AX1 (arabinoxylan), LM27 (grass heteroxylan), LM28 (glucuronoxylan), LM11 (low-substituted xylan), LM20 (esterified homogalacturonan), LM19 (un-esterified homogalacturonan), RU2 (rhamnogalacturonan I backbone), LM5 (1,4- β -galactan), LM6 (1,5- α -arabinan), and LM26 (1,6-branched 1,4- β -galactan) antibodies. Bar—100 μ m. No fluorescence was detected in negative control samples (primary antibodies were omitted) under the observation conditions.

Transcripts of many GTs present in the meristem zone exhibited a substantial increase in expression in the early elongation zone, peaked in the active elongation zone, and subsequently decreased in the late elongation zone (Fig. 8). These GTs included cellulose synthase isoforms related to PCW deposition, MLG synthases and GAX backbone and side-chain synthases, and RG-I backbone and side-chain synthases. Many of these genes were combined into one co-expression network when PCW CesAs were used as baits (Table S1). A proteomic study²² revealed the accumulation of the corresponding proteins between the apical part of the root and root hair region. In meristem region this amount was comparable with the level of XyG-related proteins. At further stages of development these proteins became the most abundant among all studied GTs (Fig. 8). Antibodies specific for polysaccharides synthesized by GTs of this cluster (BG1 for MLG; AX1 for GAX; and RU2, LM5, LM6, and

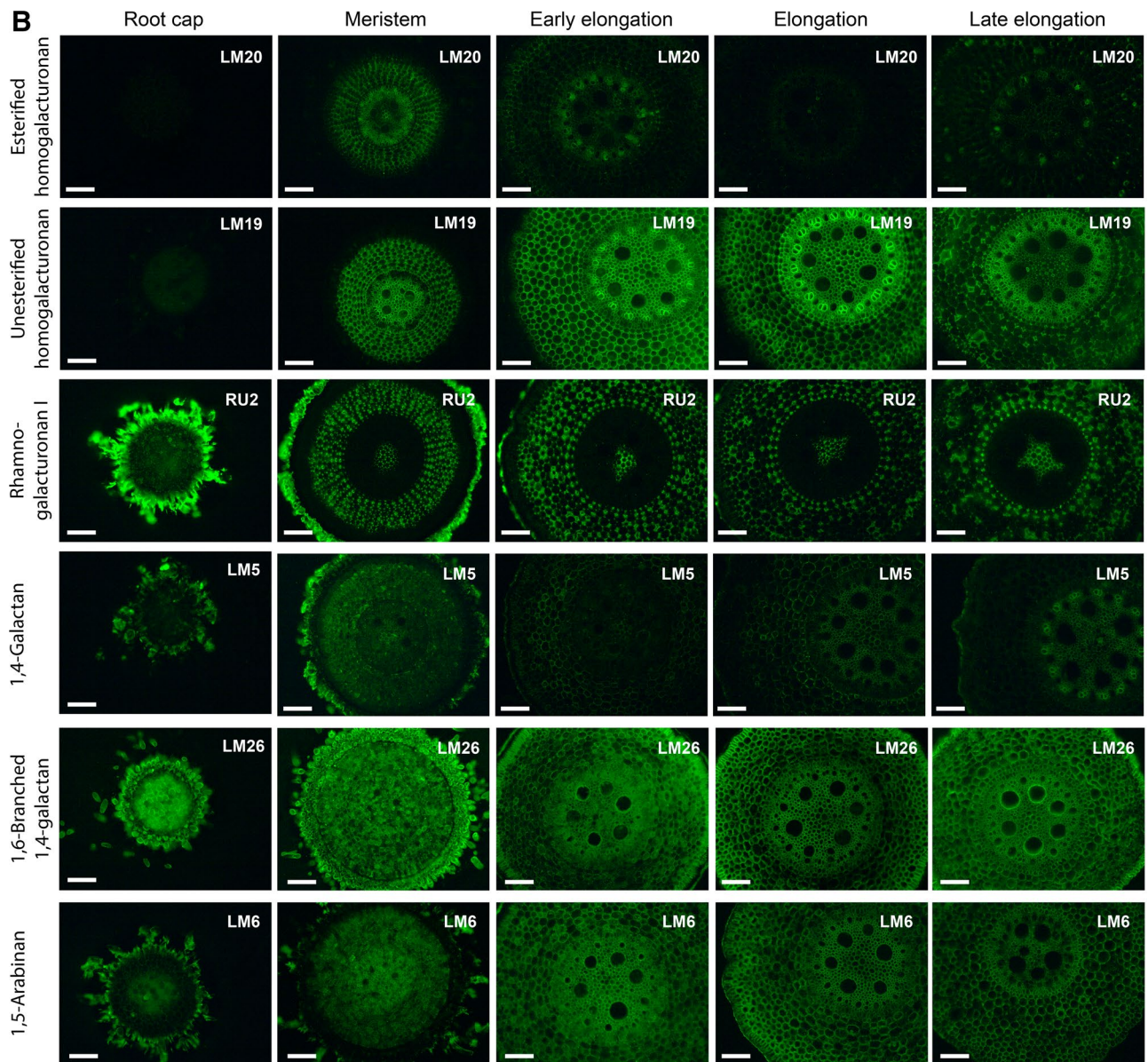


Figure 7. (continued)

LM26 for RG-I) bound the cell walls of maize root the most actively (Fig. 7). However, the labelling by BG1 and AX1 was weaker in meristem. RG-I specific probes were distributed uniformly.

Low expression in the root cap, meristem and early elongation zone and increased expression in the elongation and late elongation zones were characteristics of the fourth major pattern of GT expression (Fig. 8). *CesAs* responsible for secondary cell wall formation and many GAX-related synthases were pooled into this cluster and into one co-expression network. Corresponding proteins were specifically abundant in the stele of the root hair region of maize root²² (Fig. 8). These features of transcription and translation correlate with the development of the vascular system and SCW thickening in maize root, as visualized using Calcofluor staining and LM11, and LM28 labelling (Fig. 7).

Discussion

The type II primary cell wall is considered the characteristic feature of grasses¹. The content of XyG and pectins—the major constituents of type I primary cell walls—is usually reported to be less than 10% in grass cell walls^{17,64,65}. However, both the set of expressed genes for various GTs and distribution of epitopes for numerous antibodies reveal the working machinery required to synthesize XyG and pectins (Fig. 8). The GTs implicated in XyG synthesis were actively expressed in the root cap and meristem (Fig. 5 and 8). Distinct presence of XyG was confirmed using immunolabelling (Fig. 7, LM25). Thus, the active synthesis of XyG indeed occurs at early stages of grass cell development. We suggest that XyG may be present at high levels in the walls of meristematic

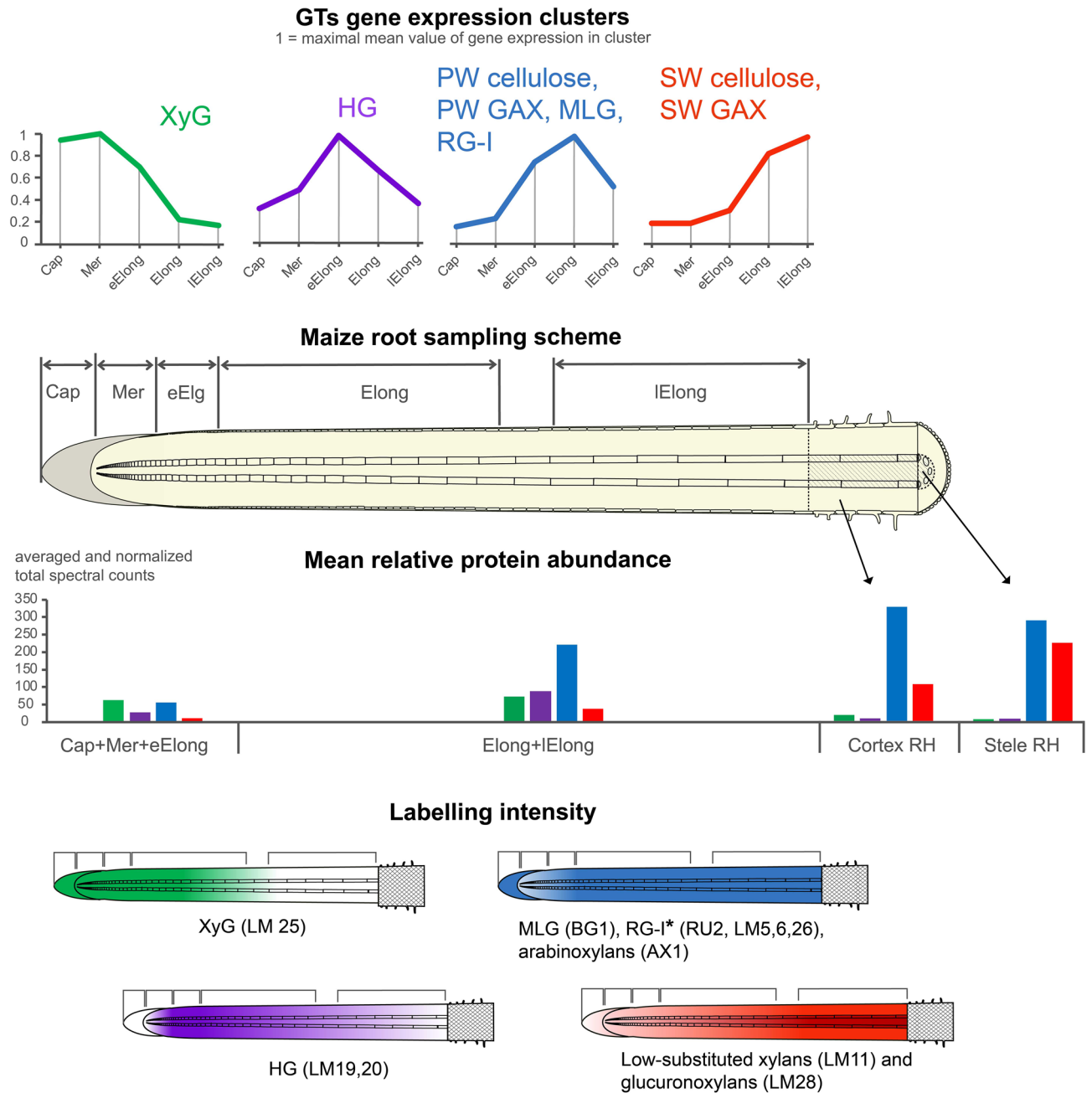


Figure 8. Four major clusters of GT expression in maize root. Expression profiles represent normalized and averaged TGR values for each cluster. Polysaccharides were assigned to a particular cluster based on the proportion of corresponding GTs included in the cluster. Protein levels are shown on a diagram as means for all members of a particular cluster. Labelling intensity is shown as color gradient where white corresponds to weak labelling. XyG—xyloglucan, HG—homogalacturonan, PW—primary cell wall, GAX—glucuronoarabinosyl, MLG—mixed-linkage glucan, RG-I—rhamnogalacturonan-I, SW—secondary cell wall. Cap—Root cap, Mer—meristem, eElong—early elongation zone, Elong—elongation zone, and IElong—late elongation zone, Cortex RH and Stele RH—cortex and stele in root hair region, respectively. *RG-I related antibodies had equal intensity of labelling in all studied root zones.

cells. Its content in coleoptiles and internodes typically used for investigations may be low since no or few dividing cells are present in these plant parts. The high XyG level may be necessary to form the required density of “biomechanical hotspots” to initiate elongation in a manner similar to dicots.

In elongation and late elongation zones of maize root the mRNA level of genes involved in XyG biosynthesis drops down, XyG labelling intensity decreases (Fig. 8). However, recent study of the maize coleoptile glycome and proteome revealed the unexpected abundance of XyGs in the Golgi apparatus that contrasted relatively low content in cell wall⁶⁵. Together with the earlier report of XyG internalization from the cell wall and transport to

the cytoplasm in maize root meristem⁶⁶, these data indicate the possibility of XyG recycling in elongating cells. The circulation of XyGs that were initially synthesized at the stage of division may provide each new layer of the cell wall with a sufficient amount of XyG-based “biomechanical hotspots” if they are necessary for elongation growth. However, supposing XyG-based “biomechanical hotspots” indeed mediate an elongation growth of grass cells, it is unclear why α -expansins have no substantial effect on the creep of plants with the type II cell walls⁶⁷. The clue may be the fact that β -expansin clade did not replace α -expansins in grass genomes but was developed additionally⁶⁷. As an assumption, the coordinative action of these two expansin families may be necessary to induce elongation.

HG is another component typical for type I cell walls which presence may affect the architecture of grass cell walls. The expression of many genes encoding HG backbone synthases peaked at the transition to elongation (Fig. 6 and 8). Intensive labelling by HG-recognizing antibodies was observed in meristem and early elongation zones (Fig. 7, LM19, LM20). The increased content of pectins in the meristematic region of maize root as compared to elongation zone was detected by a higher proportion of uronic acids in corresponding segments^{68,69}. We have observed a decrease in the level of HG methylation at the beginning of elongation growth (Fig. 6). In dicots, the reduction in pectin methylation correlates with increased cell wall extensibility^{70–72}. Methyl-esterified HG disappeared from maize root sections at early elongation stage, while un-esterified HG persisted for a longer time (Fig. 7, LM19, LM20). To our knowledge, this study is the first to show a change in the level of pectin methylation during the elongation growth of cereal root.

Along with the level of methyl-esterification of HGs, the type and relative abundance of RG-I side-chains may modulate cell wall mechanics^{62,73,74}. Basically, a higher level of side-chains and higher branching degree correspond to a more elastic cell wall. This increase in elasticity is proposed to be the consequence of pectins high water-holding capacity and ability to provide the properties of fluid-saturated poro-elastic material to cell walls⁴.

RG-I related genes were co-expressed with primary cell wall cellulose synthases and MLG synthases, with the peak expression observed at the stage of active elongation. Immunolabelling with the corresponding antibodies was more or less uniform along the root length (Fig. 7, RU-2, LM5, LM26, and LM6).

Based on these findings, the machinery necessary to generate the set of components for the type I primary cell wall operates in growing maize root. Thus, the basic mechanisms of cell wall surface enlargement involving XyGs, HGs and RGs-I may be valid for plant species with both types of primary cell walls.

GAX and MLG are the renowned constituents of the primary cell wall of grasses¹. What privileges do they provide to the plant organism, if the basic mechanism for cell enlargement may be established in grasses in a similar manner to dicots?

The maximum expression of transcripts encoding MLG synthases (ZmCslFs) was observed in the active elongation stage of root development (Fig. 8), and these synthases were co-expressed with primary cell wall-related cellulose synthases (Fig. 3 and Table S1). Together with long-lasting idea of MLG importance for cell expansion^{7,64,75–77}, this polymer is currently often considered a short-term storage of glucose independent of starch metabolism⁷⁸. Any impediment to MLG turnover may decrease the energy supply, what explains some previously reported findings, such as the increased turnover of MLG during rapid cell growth^{79,80} or inhibition of auxin-induced growth by antibodies that bind MLG or MLG-degrading enzymes, preventing the hydrolysis of this polysaccharide^{81,82}. Thus, MLG may combine the functions of the reserve and a filler of the space between cellulose microfibrils during their movement away from each other in the course of cell elongation.

Representative members of GT families involved in GAX biosynthesis are expressed differently (Figs. 3, 4, 8). Some of these genes display transcriptional and translational profiles similar to primary cell wall cellulose synthases, while the others are co-expressed with secondary cell wall cellulose synthases (Fig. 8 and Table S1). Homologous genes displaying altered expression according to two these profiles were detected in GT families engaged in the biosynthesis of both the backbone and side-chains of GAX. Thus, two separate gene sets may be responsible for the biosynthesis of GAX for primary and secondary cell wall deposition in maize root (Figs. 3 and 4). Further diversity of GAX molecules in cell walls of maize root is evidenced by the accumulation of LM27 epitope specifically in rhizodermal and cortical cells (Fig. 7). This epitope is not yet characterized, but is presumed to be a complex substitution of grass heteroxylans⁵⁶. Complex GAX are thought to be important for the formation of hemicellulose:lignin complexes, cessation of growth, and in defense mechanisms⁸³.

G(A)Xs of the maize root primary cell wall and secondary cell walls of dicots have specific domains^{84,85} (Fig. 1). Different parts of these molecules have different patterns of backbone substitution and different abilities to interact with cellulose⁸⁶. Therefore, one molecule may serve as both bonding agent and spacer for cellulose microfibrils, as it is suggested in the models of grass cell wall^{7,13}.

Thus, MLG and GAX presence may provide increased diversity, domain structure, and/or additional functions; however, these properties do not directly explain their importance in elongation growth per se. This importance is strongly suggested by the dynamics of MLGs and GAXs accumulation. Both these polymers exist in cell walls of maize root already in meristem, but account just a few percent of cell wall weight^{85,87}. Cell walls of quiescent center of maize root are totally free of MLG, as was demonstrated by immunocytochemistry⁸⁷. The proportion of MLGs and GAXs within cell walls increases gradually from meristem to late elongation zone; at active elongation stage these polysaccharides characteristic of type II cell walls become dominating. Besides, one of the well-documented modifications of type II primary cell walls during elongation growth is the decrease in GAX substitution with arabinose^{64,77,80}, which may alter the domain proportion and modify the GAX:cellulose interactions⁷. The dynamics of arabinofuranosidase gene transcription and corresponding activity in the crude extracts gradually increases from the meristem to late elongation zones⁸⁸, indicating the involvement of GAX modification in some steps of elongation process. And still, there is no sufficient information to answer the question on the privileges obtained by grasses due to the presence of GAX and MLG.

Polysaccharide ensemble of cell walls in maize root is dynamically changed in the course of elongation growth. At earlier stages of development, components characteristic of type I primary cell walls are actively deposited.

Type II specific polysaccharides exist in cell walls of maize root already in the meristem; however, they become dominating only when the elongation rate reaches a maximum. Growth cessation is coupled to the diversification of GAX molecules in cell walls of different tissues. Mechanisms of elongation growth in grasses are still far from understanding. However, new participants of this process revealed by a transcriptomic approach should now be taken into account.

Materials and methods

Plant material and sample preparation. Investigations were conducted with the roots of 4-day-old maize seedlings (*Zea mays* L., cv. Mashuk (Niva Tatarstana, Kazan, Russia)) grown in the dark at 27 °C. The primary root was subdivided into the zones according to the following pattern: root cap, meristem (0–1 mm), early elongation (1–2 mm), elongation (2–6 mm), and late elongation (7–11 mm) as was described in Kozlova et al.⁷ and Kozlova et al.⁸⁹ (Fig. 2). The 7–11 mm root zone was renamed from post-elongation to late elongation zone in this study.

RNA extraction and sequencing. Root zones pooled from 30 plants (an average) were collected separately into plastic tubes with liquid nitrogen and stored at –80 °C. Total RNA was isolated from plant samples using the Trizol extraction method combined with RNeasy Plant Mini Kit (Qiagen) according to the manufacturer's instructions. Residual DNA was eliminated by treating the samples with DNase I using the DNA-free kit (Ambion). The RNA quantity and quality were confirmed spectrophotometrically with a NanoDrop ND-1000 spectrophotometer (Thermo Fisher Scientific) and using 1% agarose gel electrophoresis. For whole-transcriptome sequencing, cDNA libraries from the total RNA of root segments were prepared with a TruSeq Sample Prep Kit (Illumina) according to the manufacturer's instruction. Sequencing was performed using an Illumina HiSeq 2500 instrument (Illumina) with single-end 60 bp reads. Data in the form of raw reads and sample preparation descriptions were deposited at NCBI Sequence Read Archive (SRA) and are available at BioProject ID PRJNA639682. All samples were analyzed using RNA-Seq analysis in two independent biological replicates.

Processing and analysis of the RNA-Seq data. Processing and Analysis of the RNA-Seq Data were as described before by Gorshkov et al.⁹⁰. Adapter removal, quality trimming, and the removal of contaminating sequences, such as rRNAs, tRNAs, snRNAs and snoRNAs, found in the RNACentral DB⁹¹ were performed using the BBDuk utility of BBToolsv37.02 [BBTools, <https://jgi.doe.gov/data-and-tools/bbtools/bb-tools-user-guide/bbduk-guide/> (accessed on 21 January 2019)]. Clean reads for each sample were mapped onto the maize genome sequence using HISAT2 v2.1.083⁹² with the default parameters. The assembly and annotation of a reference genome of maize B73 RefGen_v4 were downloaded from Gramene (https://ensembl.gramene.org/Zea_mays/Info/Index). The read count for each gene was quantified using StringTie v2.0 software⁹³ with the default settings. For each gene, total gene reads (TGRs) were determined as the number of all reads that mapped to this gene.

The R (<https://www.R-project.org/>;95) package DESeq2 v.1.14.1⁹⁵ was used to perform the differential expression analysis of mRNAs from all samples using the TGR counts generated for each sample, as described above. The DESeq estimateSizeFactors and estimateDispersions functions (with the default options) were used to obtain normalization factors for each sample and to normalize the TGR counts. Genes with an average normalized TGR of > 16 in at least in one sample were considered as expressed, according to the recommendations of the sequencing quality control project⁹⁶. The resulting dataset consisted of 26,661 genes that were used for the differential expression analysis.

Identification of genes coding enzymes involved in cell wall polysaccharide biosynthesis. Predicted full-length protein sequences of different glycosyltransferase (GT) families and methyltransferases were recognized according to presence of characteristic domains and obtained from the Ensembl plants database (<https://plants.ensembl.org/index.html>;98) for maize, *Triticum aestivum*, and *Sorghum bicolor* genes and for one rice gene. The Phytozome v12.1 database (<https://phytozome.jgi.doe.gov/pz/portal.html>;99) was used to obtain *Arabidopsis thaliana* and rice protein sequences. The canonical transcripts were used. Genes of different GT families were recognized by the presence of the following domains: PF03552, PF00535, PF13632—GT2, PF01501—GT8, PF00777—GT29, PF01762—GT31, PF055637—GT34, PF03254—GT37, PF03360—GT43, PF03016—GT47, PF02364, PF14288—GT48, PF04577—GT61, PF01697—GT92, and PF10250—GT106. Methyltransferases belonging to 29th family were recognized by the presence of a PF03141 domain. Genes that were too short or possessed additional domains were excluded from the analysis.

Phylogenetic analysis. The retrieved maize, *Arabidopsis*, and rice (wheat and *Sorghum* in some cases) amino acid sequences were subjected to multiple alignment using the web-based services Clustal Omega (<https://www.ebi.ac.uk/Tools/msa/clustalo>,100) and Muscle (<https://www.ebi.ac.uk/Tools/msa/muscle>,100). The satisfactory alignments were chosen and subjected to a maximum likelihood phylogenetic analysis which was performed using IQTREE1.6.9 software¹⁰⁰. The best-fit model of sequence evolution was selected using Akaike Information Criterion (AIC) and Bayesian Information Criterion (BIC) implemented in ModelFinder (IQTREE1.6.9)¹⁰¹ and the ultrafast bootstrap branch support with 10,000 replicates¹⁰² was used to construct each dendrogram. Trees were visualized using the web-based service iTOL 5.3 (<https://itol.embl.de/>;104).

Clustering and co-expression analyses. The gene co-expression was analyzed with the Comparative Co-Expression Network Construction and Visualization tool (CoExpNetViz) using the Pearson correlation

coefficient¹⁰⁴. The averaged normalized TGR values (TGR > 16 in at least one sample) were used as the input file. Genes were considered co-expressed if their correlation was greater than the 95th percentile of the correlation distribution between samples of genes per gene expression matrix. The network was visualized using Cytoscape version 3.7.2¹⁰⁵. The normalized values of expression were used to cluster recognized GTs using functions from different R packages (cluster, factoextra, and dendextend) (<https://www.R-project.org/95>). The Euclidean distance and the Pearson correlation coefficients were used to group the samples and to scale and group the genes, respectively. The Ward.D2 method was used in both cases.

Proteomic data processing. Tissue-specific expression of proteins in primary maize root has been determined by Marcon et al.²². Normalized and averaged data are available at Maize Genetics and Genomics Database (<https://www.maizegdb.org/>) and as supplemental material in Walley et al.¹⁰⁶. Data conversion from B73_RefGen_v3 to B73_RefGen_v4 coordinates was accomplished in R software environment (<https://www.R-project.org/95>) by using maize.v3TOv4.geneIDhistory.txt file, which was downloaded from <ftp://ftp.gramene.org/>. Data on GT expression were separated by gene numbers and are presented in Table S1.

Immunohistochemistry. Dissected maize roots were incubated for 1 h with 4% (w/v) paraformaldehyde prepared in 0.2 M phosphate-buffered saline (PBS, pH 7.2). Root fragments were embedded in 3% (w/v) low melting point agarose. Cross Sects. (50 μm thick) were prepared using a Leica VT 1000S (Leica Biosystems) vibratome (blade speed—0.65 mm s^{-1} , blade frequency—70 Hz for the meristem, early elongation and elongation zones; blade speed—0.225 mm s^{-1} , blade frequency—100 Hz for late elongation zone). Immunohistochemical analysis of cell wall polymers was performed using BG1 (Australian Biosupplies Pty Ltd.), AX1, RU2 (INRA), LM5, LM6, LM11, LM19, LM20, LM25, LM26, LM27, and LM28 (Leeds University) antibodies. For immunolocalization, the sections were (1) blocked with 0.2 M PBS containing 2% (w/v) bovine serum albumin (BSA) for 30 min at room temperature, (2) incubated with one of the primary monoclonal antibodies diluted 1:5 (LM5, LM6, LM11, LM19, LM20, LM25, LM26, LM27, and LM28), 1:10 (BG1) or 1:3 (AX1 and RU2) for 1.5 h at room temperature then washed three times with PBS. (3) Next, the sections were incubated with secondary anti-rat (LM5, LM6, LM11, LM19, LM20, LM25, LM26, LM27, and LM28) or anti-mouse (BG1, AX1, and RU2) IgG linked to fluorescein isothiocyanate (FITC) diluted 1:100 in PBS for 1 h at room temperature in the dark. The primary antibody treatment was omitted for the negative controls. After incubations with the antibodies, the sections were washed four times with PBS and twice with water. For the visualization of the tissue structure, sections were incubated in Calcofluor White 1:100 solution in PBS. Sections were observed using a Leica DM1000 epifluorescence microscope (Leica Biosystems) fitted with a mercury lamp. Sections were observed under epifluorescence settings with the excitation filter BP 480/40 nm and barrier filter BP527/30 nm for FITC-conjugated antibodies, and excitation filter 355–425 nm and barrier filter 470 nm for Calcofluor. All analyses were performed using at least three biological replicates. Antibodies used in the present study are listed in Table S2.

Data availability

All materials, data, and associated protocols are promptly available to readers without undue qualifications.

Received: 6 April 2020; Accepted: 12 June 2020

Published online: 02 July 2020

References

1. Carpita, N. C. & Gibeaut, D. M. Structural models of primary-cell walls in flowering plants—consistency of molecular-structure with the physical-properties of the walls during growth. *Plant J.* **3**, 1–30. <https://doi.org/10.1111/j.1365-313X.1993.tb00007.x> (1993).
2. Cosgrove, D. J. Diffuse growth of plant cell walls. *Plant Physiol.* **176**, 16–27. <https://doi.org/10.1104/pp.17.01541> (2018).
3. Park, Y. B. & Cosgrove, D. J. A revised architecture of primary cell walls based on biomechanical changes induced by substrate-specific endoglucanases. *Plant Physiol.* **158**, 1933–1943. <https://doi.org/10.1104/pp.111.192880> (2012).
4. Bidhendi, A. J. & Geitmann, A. Relating the mechanics of the primary plant cell wall to morphogenesis. *J. Exp. Bot.* **67**, 449–461. <https://doi.org/10.1093/jxb/erv535> (2016).
5. Hocq, L., Pelloux, J. & Lefebvre, V. Connecting homogalacturonan-type pectin remodeling to acid growth. *Trends Plant Sci.* **22**, 20–29. <https://doi.org/10.1016/j.tplants.2016.10.009> (2017).
6. Buckeridge, M. S., Rayon, C., Urbanowicz, B., Tiné, M. A. S. & Carpita, N. C. Mixed linkage (1 \rightarrow 3), (1 \rightarrow 4)- β -D-glucans of grasses. *Cereal. Chem.* **81**, 115–127 (2004).
7. Kozlova, L. V., Ageeva, M. V., Ibragimova, N. N. & Gorshkova, T. A. Arrangement of mixed-linkage glucan and glucuronoarabinoxylan in the cell walls of growing maize roots. *Ann. Bot.-Lond.* **114**, 1135–1145. <https://doi.org/10.1093/aob/mcu125> (2014).
8. Wang, T., Chen, Y. N., Tabuchi, A., Cosgrove, D. J. & Hong, M. The target of beta-expansin EXPB1 in maize cell walls from binding and solid-state NMR studies. *Plant Physiol.* **172**, 2107–2119. <https://doi.org/10.1104/pp.16.01311> (2016).
9. Kiemle, S. N. et al. Role of (1,3)(1,4)-beta-Glucan in cell walls: Interaction with cellulose. *Biomacromol* **15**, 1727–1736. <https://doi.org/10.1021/bm5001247> (2014).
10. Mikkelsen, D., Flanagan, B. M., Wilson, S. M., Bacic, A. & Gidley, M. J. Interactions of arabinoxylan and (1,3)(1,4)-beta-Glucan with cellulose networks. *Biomacromol* **16**, 1232–1239. <https://doi.org/10.1021/acs.biomac.5b00009> (2015).
11. Cosgrove, D. J. Loosening of plant cell walls by expansins. *Nature* **407**, 321–326. <https://doi.org/10.1038/35030000> (2000).
12. Li, L.-C., Bedinger, P. A., Volk, C., Jones, A. D. & Cosgrove, D. J. Purification and characterization of four β -expansins (Zea m1 isoforms) from maize pollen. *Plant Physiol.* **132**, 2073–2085 (2003).
13. Kang, X. et al. Lignin-polysaccharide interactions in plant secondary cell walls revealed by solid-state NMR. *Nat. Commun.* **10**, 347. <https://doi.org/10.1038/s41467-018-08252-0> (2019).
14. Simmons, T. J. et al. Folding of xylan onto cellulose fibrils in plant cell walls revealed by solid-state NMR. *Nat. Commun.* **7**, 13902. <https://doi.org/10.1038/ncomms13902> (2016).
15. Coomey, J. H., Sibout, R. & Hazen, S. P. Grass secondary cell walls, *Brachypodium distachyon* as a model for discovery. *New Phytol.* <https://doi.org/10.1111/nph.16603> (2020).

16. Bosch, M., Mayer, C. D., Cookson, A. & Donnison, I. S. Identification of genes involved in cell wall biogenesis in grasses by differential gene expression profiling of elongating and non-elongating maize internodes. *J. Exp. Bot.* **62**, 3545–3561. <https://doi.org/10.1093/jxb/err045> (2011).
17. Zhang, Q. S. *et al.* Spatial gradients in cell wall composition and transcriptional profiles along elongating maize internodes. *BMC Plant Biol.* <https://doi.org/10.1186/1471-2229-14-27> (2014).
18. Penning, B. W., McCann, M. C. & Carpita, N. C. Evolution of the cell wall gene families of grasses. *Front. Plant Sci.* <https://doi.org/10.3389/fpls.2019.01205> (2019).
19. Esau, K. *Plant anatomy*, 2nd edn (John Wiley & Sons, New York, 1965).
20. Hochholdinger, F., Woll, K., Sauer, M. & Dembinsky, D. Genetic dissection of root formation in maize (*Zea mays*) reveals root-type specific developmental programmes. *Ann. Bot.-Lond.* **93**, 359–368. <https://doi.org/10.1093/aob/mch056> (2004).
21. Stelpflug, S. C. *et al.* An expanded maize gene expression atlas based on RNA sequencing and its use to explore root development. *Plant Genome Us* <https://doi.org/10.3835/plantgenome2015.04.0025> (2016).
22. Marcon, C. *et al.* A high-resolution tissue-specific proteome and phosphoproteome atlas of maize primary roots reveals functional gradients along the root axes. *Plant Physiol.* **168**, 233. <https://doi.org/10.1104/pp.15.00138> (2015).
23. Little, A. *et al.* Revised phylogeny of the cellulose synthase gene superfamily: insights into cell wall evolution. *Plant Physiol.* **177**, 1124–1141. <https://doi.org/10.1104/pp.17.01718> (2018).
24. Amos, R. A. & Mohnen, D. Critical review of plant cell wall matrix polysaccharide glycosyltransferase activities verified by heterologous protein expression. *Front. Plant Sci.* <https://doi.org/10.3389/fpls.2019.00915> (2019).
25. Little, A. *et al.* A novel (1, 4)- β -linked glucoxylan is synthesized by members of the Cellulose synthase-like F gene family in land plants. *ACS Cent. Sci.* **5**, 73–84 (2019).
26. Urbanowicz, B. R., Pena, M. J., Moniz, H. A., Moremen, K. W. & York, W. S. Two Arabidopsis proteins synthesize acetylated xylan in vitro. *Plant J.* **80**, 197–206. <https://doi.org/10.1111/tj.12643> (2014).
27. Jensen, J. K., Johnson, N. R. & Wilkerson, C. G. Arabidopsis thaliana IRX10 and two related proteins from psyllium and *Phycomitrella patens* are xylan xylosyltransferases. *Plant J.* **80**, 207–215. <https://doi.org/10.1111/tj.12641> (2014).
28. Anders, N. *et al.* Glycosyl transferases in family 61 mediate arabinofuranosyl transfer onto xylan in grasses. *Proc. Natl. Acad. Sci. USA* **109**, 989–993. <https://doi.org/10.1073/pnas.1115858109> (2012).
29. Chiniquy, D. *et al.* Three novel rice genes closely related to the Arabidopsis IRX9, IRX9L, and IRX14 genes and their roles in xylan biosynthesis. *Front. Plant Sci.* <https://doi.org/10.3389/fpls.2013.00083> (2013).
30. Mortimer, J. C. *et al.* Absence of branches from xylan in Arabidopsis gux mutants reveals potential for simplification of lignocellulosic biomass. *Proc Natl Acad Sci USA* **107**, 17409–17414. <https://doi.org/10.1073/pnas.1005456107> (2010).
31. Zhong, R. Q., Cui, D. T., Phillips, D. R. & Ye, Z. H. A novel rice xylosyltransferase catalyzes the addition of 2-O-xylosyl side chains onto the xylan backbone. *Plant Cell Physiol.* **59**, 554–565. <https://doi.org/10.1093/pcp/pcy003> (2018).
32. Voiniciuc, C., Gunl, M., Schmidt, M. H. W. & Usadel, B. Highly branched xylan made by irregular XYLEM14 and MUCILAGE-RELATED21 links mucilage to arabidopsis seeds. *Plant Physiol.* **169**, 2481–2495. <https://doi.org/10.1104/pp.15.01441> (2015).
33. Lee, C., Teng, Q., Zhong, R. Q. & Ye, Z. H. Arabidopsis GUX proteins are glucuronyltransferases responsible for the addition of glucuronic acid side chains onto xylan. *Plant Cell Physiol.* **53**, 1204–1216. <https://doi.org/10.1093/pcp/pcs064> (2012).
34. Rennie, E. A. *et al.* Three members of the arabidopsis glycosyltransferase family 8 Are Xylan glucuronosyltransferases. *Plant Physiol.* **159**, 1408–1417. <https://doi.org/10.1104/pp.112.200964> (2012).
35. Brennan, M. & Harris, P. J. Distribution of fucosylated xyloglucans among the walls of different cell types in monocotyledons determined by immunofluorescence microscopy. *Mol. Plant* **4**, 144–156. <https://doi.org/10.1093/mp/ssq067> (2011).
36. Liu, L. F., Paulitz, J. & Pauly, M. The presence of fucogalactoxyloglucan and its synthesis in rice indicates conserved functional importance in plants. *Plant Physiol.* **168**, 549. <https://doi.org/10.1104/pp.15.00441> (2015).
37. Pauly, M. & Keegstra, K. Biosynthesis of the plant cell wall matrix polysaccharide xyloglucan. *Annu. Rev. Plant Biol.* **67**(67), 235–259. <https://doi.org/10.1146/annurev-arplant-043015-112222> (2016).
38. Cocuron, J. C. *et al.* A gene from the cellulose synthase-like C family encodes a beta-1,4 glucan synthase. *Proc. Natl. Acad. Sci. USA* **104**, 8550–8555. <https://doi.org/10.1073/pnas.0703133104> (2007).
39. Cavalier, D. M. & Keegstra, K. Two xyloglucan xylosyltransferases catalyze the addition of multiple xylosyl residues to cel-lohexaose. *J. Biol. Chem.* **281**, 34197–34207. <https://doi.org/10.1074/jbc.M606379200> (2006).
40. Culbertson, A. T. *et al.* Enzymatic activity of xyloglucan xylosyltransferase 5. *Plant Physiol.* **171**, 1893–1904. <https://doi.org/10.1104/pp.16.00361> (2016).
41. Madson, M. *et al.* The MUR3 gene of Arabidopsis encodes a xyloglucan galactosyltransferase that is evolutionarily related to animal exostosins. *Plant Cell* **15**, 1662–1670. <https://doi.org/10.1105/tpc.009837> (2003).
42. Xu, H. *et al.* Genome-wide analysis of sorghum GT47 family reveals functional divergences of MUR3-like genes. *Front. Plant Sci.* <https://doi.org/10.3389/fpls.2018.01773> (2018).
43. Urbanowicz, B. R. *et al.* Structural, mutagenic and in silico studies of xyloglucan fucosylation in Arabidopsis thaliana suggest a water-mediated mechanism. *Plant J.* **91**, 931–949. <https://doi.org/10.1111/tj.13628> (2017).
44. Zabolina, O. A. Xyloglucan and its biosynthesis. *Front. Plant Sci.* <https://doi.org/10.3389/fpls.2012.00134> (2012).
45. Mohnen, D. Pectin structure and biosynthesis. *Curr. Opin. Plant Biol.* **11**, 266–277. <https://doi.org/10.1016/j.pbi.2008.03.006> (2008).
46. Atmodjo, M. A. *et al.* Galacturonosyltransferase (GAUT) 1 and GAUT7 are the core of a plant cell wall pectin biosynthetic homogalacturonan: galacturonosyltransferase complex. *Proc. Natl. Acad. Sci.* **108**, 20225–20230 (2011).
47. Biswal, A. K. *et al.* Working towards recalcitrance mechanisms: increased xylan and homogalacturonan production by overexpression of GalacturonosylTransferase12 (GAUT12) causes increased recalcitrance and decreased growth in Populus. *Biotechnol. Biofuels.* <https://doi.org/10.1186/s13068-017-1002-y> (2018).
48. Voiniciuc, C., Dama, M., Gawenda, N., Stritt, F. & Pauly, M. Mechanistic insights from plant heteromannan synthesis in yeast. *Proc. Natl. Acad. Sci. USA* **116**, 522–527. <https://doi.org/10.1073/pnas.1814003116> (2019).
49. Krupkova, E., Immerzeel, P., Pauly, M. & Schmulling, T. The TUMOROUS SHOOT DEVELOPMENT2 gene of Arabidopsis encoding a putative methyltransferase is required for cell adhesion and co-ordinated plant development. *Plant J.* **50**, 735–750. <https://doi.org/10.1111/j.1365-313X.2007.03123.x> (2007).
50. Mouille, G. *et al.* Homogalacturonan synthesis in Arabidopsis thaliana requires a Golgi-localized protein with a putative methyltransferase domain. *Plant J.* **50**, 605–614. <https://doi.org/10.1111/j.1365-313X.2007.03086.x> (2007).
51. Takenaka, Y. *et al.* Pectin RG-I rhamnosyltransferases represent a novel plant-specific glycosyltransferase family. *Nat. Plants* **4**, 669–676. <https://doi.org/10.1038/s41477-018-0217-7> (2018).
52. Liwanag, A. J. M. *et al.* Pectin biosynthesis: GAL51 in Arabidopsis thaliana Is a beta-1,4-Galactan beta-1,4-Galactosyltransferase. *Plant Cell* **24**, 5024–5036. <https://doi.org/10.1105/tpc.112.106625> (2012).
53. Harholt, J. *et al.* ARAD proteins associated with pectic Arabinan biosynthesis form complexes when transiently overexpressed in planta. *Planta* **236**, 115–128. <https://doi.org/10.1007/s00425-012-1592-3> (2012).
54. Meikle, P. J., Hoogenraad, N. J., Bonig, I., Clarke, A. E. & Stone, B. A. A (1- β 3,1- β 4)-beta-glucan-specific monoclonal-antibody and its use in the quantitation and immunocyto-chemical location of (1- β 3,1- β 4)-beta-glucans. *Plant J.* **5**, 1–9. <https://doi.org/10.1046/j.1365-313X.1994.5010001.x> (1994).

55. Guillon, F. *et al.* Generation of polyclonal and monoclonal antibodies against arabinoxylans and their use for immunocytochemical location of arabinoxylans in cell walls of endosperm of wheat. *J. Cereal. Sci.* **40**, 167–182. <https://doi.org/10.1016/j.jcs.2004.06.004> (2004).
56. Cornuault, V. *et al.* Monoclonal antibodies indicate low-abundance links between heteroxylan and other glycans of plant cell walls. *Planta* **242**, 1321–1334. <https://doi.org/10.1007/s00425-015-2375-4> (2015).
57. McCartney, L., Marcus, S. E. & Knox, J. P. Monoclonal antibodies to plant cell wall xylans and arabinoxylans. *J. Histochem. Cytochem.* **53**, 543–546. <https://doi.org/10.1369/jhc.4B6578.2005> (2005).
58. Pedersen, H. L. *et al.* Versatile High Resolution Oligosaccharide Microarrays for Plant Glycobiology and Cell Wall Research. *J. Biol. Chem.* <https://doi.org/10.1074/jbc.M112.396598> (2012).
59. Verherbruggen, Y., Marcus, S. E., Haeger, A., Ordaz-Ortiz, J. J. & Knox, J. P. An extended set of monoclonal antibodies to pectic homogalacturonan. *Carbohydr. Res.* **344**, 1858–1862. <https://doi.org/10.1016/j.carres.2008.11.010> (2009).
60. Ralet, M. C., Tranquet, O., Poulain, D., Moise, A. & Guillon, F. Monoclonal antibodies to rhamnogalacturonan I backbone. *Planta* **231**, 1373–1383. <https://doi.org/10.1007/s00425-010-1116-y> (2010).
61. Jones, L., Seymour, G. B. & Knox, J. P. Localization of pectic galactan in tomato cell walls using a monoclonal antibody specific to (1->4)-beta-D-galactan. *Plant Physiol.* **113**, 1405–1412. <https://doi.org/10.1104/pp.113.4.1405> (1997).
62. Torode, T. A. *et al.* Branched pectic galactan in phloem-sieve-element cell walls: implications for cell mechanics. *Plant Physiol.* **176**, 1547–1558. <https://doi.org/10.1104/pp.17.01568> (2018).
63. Willats, W. G. T., Marcus, S. E. & Knox, J. P. Generation of a monoclonal antibody specific to (1->5)-alpha-L-arabinan. *Carbohydr. Res.* **308**, 149–152. [https://doi.org/10.1016/S0008-6215\(98\)00070-6](https://doi.org/10.1016/S0008-6215(98)00070-6) (1998).
64. Gibeaut, D. M., Pauly, M., Bacic, A. & Fincher, G. B. Changes in cell wall polysaccharides in developing barley (*Hordeum vulgare*) coleoptiles. *Planta* **221**, 729–738. <https://doi.org/10.1007/s00425-005-1481-0> (2005).
65. Okekeogbu, I. O. *et al.* Glycome and proteome components of golgi membranes are common between two angiosperms with distinct cell-wall structures. *Plant Cell* **31**, 1094–1112. <https://doi.org/10.1105/tpc.18.00755> (2019).
66. Baluška, F. *et al.* Cell wall pectins and xyloglucans are internalized into dividing root cells and accumulate within cell plates during cytokinesis. *Protoplasma* **225**, 141–155 (2005).
67. Sampedro, J., Guttman, M., Li, L. C. & Cosgrove, D. J. Evolutionary divergence of beta-expansin structure and function in grasses parallels emergence of distinctive primary cell wall traits. *Plant J.* **81**, 108–120. <https://doi.org/10.1111/tpj.12715> (2015).
68. Dever, J. E., Bandurski, R. S. & Kivilaan, A. Partial chemical characterization of corn root cell walls. *Plant Physiol.* **43**, 50–56 (1968).
69. Eticha, D., Stass, A. & Horst, W. J. Localization of aluminium in the maize root apex: Can morin detect cell wall-bound aluminium? *J. Exp. Bot.* **56**, 1351–1357. <https://doi.org/10.1093/jxb/eri136> (2005).
70. Daher, F. B. *et al.* Anisotropic growth is achieved through the additive mechanical effect of material anisotropy and elastic asymmetry. *Elife* **7**, e38161 (2018).
71. Peaucelle, A. *et al.* Pectin-induced changes in cell wall mechanics underlie organ initiation in Arabidopsis. *Curr. Biol.* **21**, 1720–1726. <https://doi.org/10.1016/j.cub.2011.08.057> (2011).
72. Peaucelle, A., Wightman, R. & Hofte, H. The control of growth symmetry breaking in the Arabidopsis hypocotyl. *Curr. Biol.* **25**, 1798. <https://doi.org/10.1016/j.cub.2015.06.032> (2015).
73. Majda, M. *et al.* Mechanochemical polarization of contiguous cell walls shapes plant pavement cells. *Dev. Cell* **43**, 290. <https://doi.org/10.1016/j.devcel.2017.10.017> (2017).
74. Ulvskov, P. *et al.* Biophysical consequences of remodeling the neutral side chains of rhamnogalacturonan I in tubers of transgenic potatoes. *Planta* **220**, 609–620. <https://doi.org/10.1007/s00425-004-1373-8> (2005).
75. Luttenegger, D. G. & Nevins, D. J. Transient nature of a (1-3), (1-4)-Beta-D-Glucan in Zea-Mays coleoptile cell-walls. *Plant Physiol.* **77**, 175–178. <https://doi.org/10.1104/pp.77.1.175> (1985).
76. Carpita, N. C. Cell-wall development in maize coleoptiles. *Plant Physiol.* **76**, 205–212. <https://doi.org/10.1104/pp.76.1.205> (1984).
77. Obel, N., Porchia, A. C. & Scheller, H. V. Dynamic changes in cell wall polysaccharides during wheat seedling development. *Phytochemistry* **60**, 603–610. [https://doi.org/10.1016/S0031-9422\(02\)00148-6](https://doi.org/10.1016/S0031-9422(02)00148-6) (2002).
78. Bulone, V., Schwerdt, J. G. & Fincher, G. B. Co-evolution of enzymes involved in plant cell wall metabolism in the grasses. *Front. Plant Sci.* <https://doi.org/10.3389/fpls.2019.01009> (2019).
79. Inouhe, M. & Nevins, D. J. Inhibition of auxin-induced cell elongation of maize coleoptiles by antibodies specific for cell-wall glucanases. *Plant Physiol.* **96**, 426–431. <https://doi.org/10.1104/pp.96.2.426> (1991).
80. Gibeaut, D. M. & Carpita, N. C. Tracing cell-wall biogenesis in intact-cells and plants—selective turnover and alteration of soluble and cell-wall polysaccharides in grasses. *Plant Physiol.* **97**, 551–561. <https://doi.org/10.1104/pp.97.2.551> (1991).
81. Hoson, T. & Nevins, D. J. Effect of anti-wall protein antibodies on auxin-induced elongation, cell-wall loosening, and beta-D-glucan degradation in maize coleoptile segments. *Physiol. Plant* **77**, 208–215. <https://doi.org/10.1111/j.1399-3054.1989.tb04971.x> (1989).
82. Hoson, T. & Nevins, D. J. Beta-D-glucan antibodies inhibit auxin-induced cell elongation and changes in the cell-wall of Zea coleoptile segments. *Plant Physiol.* **90**, 1353–1358. <https://doi.org/10.1104/pp.90.4.1353> (1989).
83. Saulnier, L. Types and functionality of polysaccharides in cereal grains. *Food Chem. Funct. Anal.* **6**, 54–84. <https://doi.org/10.1039/9781788012799> (2019).
84. Bromley, J. R. *et al.* GUX 1 and GUX 2 glucuronyltransferases decorate distinct domains of glucuronoxylan with different substitution patterns. *Plant J.* **74**, 423–434 (2013).
85. Kozlova, L. V., Mikshina, P. V. & Gorshkova, T. A. Glucuronoarabinoxylan extracted by treatment with endoxylanase from different zones of growing maize root. *Biochem. Moscow* **77**, 395–403. <https://doi.org/10.1134/S0006297912040116> (2012).
86. Busse-Wicher, M. *et al.* Evolution of xylan substitution patterns in gymnosperms and angiosperms: implications for xylan interaction with cellulose. *Plant Physiol.* **171**, 2418–2431. <https://doi.org/10.1104/pp.16.00539> (2016).
87. Kozlova, L., Snegireva, A. & Gorshkova, T. Distribution and structure of mixed linkage glucan at different stages of elongation of maize root cells. *Russ. J. Plant Phys.* **59**, 339–347 (2012).
88. Kozlova, L. V., Gorshkov, O. V., Mokshina, N. E. & Gorshkova, T. A. Differential expression of alpha-L-arabinofuranosidases during maize (*Zea mays* L.) root elongation. *Planta* **241**, 1159–1172 (2015).
89. Kozlova, L. V., Gorshkov, O. V., Mokshina, N. E. & Gorshkova, T. A. Differential expression of alpha-L-arabinofuranosidases during maize (*Zea mays* L.) root elongation. *Planta* **241**, 1159–1172. <https://doi.org/10.1007/s00425-015-2244-1> (2015).
90. Gorshkov, O. *et al.* Intrusive growth of phloem fibers in flax stem: integrated analysis of miRNA and mRNA expression profiles. *Plants Basel.* <https://doi.org/10.3390/plants8020047> (2019).
91. Petrov, A. I. *et al.* RNACentral: A comprehensive database of non-coding RNA sequences. *Nucleic Acids Res.* **45**, D128–D134. <https://doi.org/10.1093/nar/gkw1008> (2017).
92. Kim, D., Landmead, B. & Salzberg, S. L. HISAT: A fast spliced aligner with low memory requirements. *Nat. Methods* **12**, 357–U121. <https://doi.org/10.1038/Nmeth.3317> (2015).
93. M Pertea, D Kim, GM Pertea, JT Leek, SL Salzberg (2016) Transcript-level expression analysis of RNA-seq experiments with HISAT StringTie and Ballgown. *Nat. Protoc.* **11**, 1650–1667. <https://doi.org/10.1038/nprot.2016.095>
94. Team, R. C. R: A Language and Environment for Statistical Computing (2013).

95. Love, M. I., Huber, W. & Anders, S. Moderated estimation of fold change and dispersion for RNA-seq data with DESeq2. *Genome Biol.* <https://doi.org/10.1186/s13059-014-0550-8> (2014).
96. Su, Z. Q. *et al.* A comprehensive assessment of RNA-seq accuracy, reproducibility and information content by the Sequencing Quality Control Consortium. *Nat. Biotechnol.* **32**, 903–914. <https://doi.org/10.1038/nbt.2957> (2014).
97. Bolser, D., Staines, D. M., Pritchard, E. & Kersey, P. In *Plant Bioinformatics* 115–140 (Springer, 2016).
98. Goodstein, D. M. *et al.* Phytozome: A comparative platform for green plant genomics. *Nucleic Acids Res.* **40**, D1178–D1186 (2012).
99. Madeira, F. *et al.* The EMBL-EBI search and sequence analysis tools APIs in 2019. *Nucleic Acids Res.* **47**, W636–W641 (2019).
100. Nguyen, L.-T., Schmidt, H. A., Von Haeseler, A. & Minh, B. Q. IQ-TREE: a fast and effective stochastic algorithm for estimating maximum-likelihood phylogenies. *Mol. Biol. Evol.* **32**, 268–274 (2015).
101. Kalyaanamoorthy, S., Minh, B. Q., Wong, T. K. F., von Haeseler, A. & Jermini, L. S. ModelFinder: fast model selection for accurate phylogenetic estimates. *Nat. Methods* **14**, 587–589. <https://doi.org/10.1038/nmeth.4285> (2017).
102. Minh, B. Q., Nguyen, M. A. T. & von Haeseler, A. Ultrafast approximation for phylogenetic bootstrap. *Mol. Biol. Evol.* **30**, 1188–1195. <https://doi.org/10.1093/molbev/mst024> (2013).
103. Letunic, I. & Bork, P. Interactive Tree Of Life (iTOL) v4: Recent updates and new developments. *Nucleic Acids Res.* **47**, W256–W259. <https://doi.org/10.1093/nar/gkz239> (2019).
104. Tzfadia, O. *et al.* CoExpNetViz: Comparative co-expression networks construction and visualization tool. *Front. Plant Sci.* <https://doi.org/10.3389/fpls.2015.01194> (2016).
105. Shannon, P. *et al.* Cytoscape: A software environment for integrated models of biomolecular interaction networks. *Genome Res.* **13**, 2498–2504. <https://doi.org/10.1101/gr.1239303> (2003).
106. Walley, J. W. *et al.* Integration of omic networks in a developmental atlas of maize. *Science* **353**, 814–818. <https://doi.org/10.1126/science.aag1125> (2016).

Acknowledgements

We would like to express our gratitude to Professor Paul Knox (University of Leeds, UK) and Dr Marie-Christine Ralet (French National Institute for Agricultural Research, Nantes, France) for kindly providing the antibodies used in this study. The study was partially funded by the Russian Scientific Foundation, project # 18-14-00168 (Liudmila Kozlova, Alsu Nazipova, Oleg Gorshkov and Anna Petrova). We also acknowledge financial support from the government assignment for FRC Kazan Scientific Center of RAS (Tatyana Gorshkova).

Author contributions

L.K., A.P. and T.G. conceived and designed the study. L.K., A.N., O.G. and A.P. performed the experiments and analyzed the data. A.N., L.K. and T.G. wrote the manuscript. Illustrations are prepared by A.N. (Fig. 1–6, 8) and A.P. (Fig. 7). All authors reviewed and approved the manuscript.

Competing interests

The authors declare no competing interests.

Additional information

Supplementary information is available for this paper at <https://doi.org/10.1038/s41598-020-67782-0>.

Correspondence and requests for materials should be addressed to L.V.K.

Reprints and permissions information is available at www.nature.com/reprints.

Publisher's note Springer Nature remains neutral with regard to jurisdictional claims in published maps and institutional affiliations.



Open Access This article is licensed under a Creative Commons Attribution 4.0 International License, which permits use, sharing, adaptation, distribution and reproduction in any medium or format, as long as you give appropriate credit to the original author(s) and the source, provide a link to the Creative Commons license, and indicate if changes were made. The images or other third party material in this article are included in the article's Creative Commons license, unless indicated otherwise in a credit line to the material. If material is not included in the article's Creative Commons license and your intended use is not permitted by statutory regulation or exceeds the permitted use, you will need to obtain permission directly from the copyright holder. To view a copy of this license, visit <http://creativecommons.org/licenses/by/4.0/>.

© The Author(s) 2020